THESIS

COLD POOL TRAIN DYNAMICS AND TRANSPORT

Submitted by

Christine Allison Neumaier

Department of Atmospheric Science

In partial fulfillment of the requirements

For the Degree of Master of Science

Colorado State University

Fort Collins, Colorado

Fall 2023

Master's Committee:

Advisor: Susan C. van den Heever
Co-Advisor: Leah D. Grant

Sonia M. Kreidenweis
Subhas K. Venayagamoorthy

ABSTRACT

COLD POOL TRAIN DYNAMICS AND TRANSPORT

Convectively generated cold air outflows, referred to as cold pools, can initiate new convection and loft aerosols, such as dust or pollen. In the BioAerosols and Convective Storms Phase I (BACS-I) field campaign, we observed multiple cold pools passing over the same location on the same day, without colliding, which we refer to as a "cold pool train". The goals of this study are to examine how the dynamics of cold pools in a cold pool train differ, how cold pools in a cold pool train affect the vertical distribution of aerosols, and how the results may change if the properties of the second cold pool change. We utilize idealized simulations of a cold pool train composed of two cold pools to investigate the dynamics of the cold pools in the train and how cold pool trains loft and transport aerosols. We test the sensitivity of the second cold pool's evolution and aerosol lofting to its initial temperature deficit and timing relative to the first cold pool, based on the cold pool trains observed during BACS-I. Passive tracers are initialized at different times to represent the background aerosols present before cold pools, aerosols newly emitted after the passage of the first cold pool in the train, and aerosols within and ahead of each cold pool, to distinguish between how cold pools loft their own air compared to distinct environmental air.

We find that the first cold pool (CP1) in the cold pool train stably stratifies the environment ahead of the *downshear* side of the second cold pool (CP2) in the train. All else equal, this stabilization acts to decrease the height of CP2's head and increase its propagation speed. However, the stratification also increases the horizontal wind shear ahead of CP2 by

decreasing the lower level wind speeds, which opposes the stability effects and acts to deepen the head of CP2. In the CONTROL case, where CP2 is initialized two hours after CP1 and with the same temperature deficit as CP1, we find that the wind profile plays a more dominant role for the dynamics of CP2 because overall, CP2's head is deeper and propagates slower compared to CP1. In the temperature deficit sensitivity experiments, we find that CP2's head depth and propagation speed decreases with decreasing temperature deficit. Finally, in the timing sensitivity tests of CP2, we find CP2 initiated 90 minutes after CP1 had the deepest head, while CP2 in the CONTROL (120 minutes) experiment propagated the slowest.

Our analysis of the tracer lofting mechanisms in the simulations shows that the *downshear* leading edge of CP1 lofts the highest concentration of *background* aerosol, while the downshear leading edge of the CONTROL CP2 lofts less than half of the amount of background aerosol as CP1. However, the downshear leading edge of CP2 lofts more than double the concentration of *newly emitted* aerosol compared to the background aerosol lofted by CP1. The atmospheric stratification left behind by CP1 acts to trap the newly emitted aerosol near the surface, leading to greater concentrations lofted compared to the background aerosol which is well mixed in the boundary layer. Analysis of the tracers initialized within and ahead of the cold pools demonstrates that the lofted aerosol primarily originates from the air ahead of the cold pools, while the aerosol originating in the cold pools remains trapped within the cold pools. The CONTROL CP2 lofts the most aerosol of the temperature deficit sensitivity tests, and the CONTROL CP2, released the farthest apart temporally from CP1, lofts the most aerosol out of the timing sensitivity tests. Therefore, while the wind profile change ahead of CP2 plays a dominant role in its dynamics, atmospheric static stabilization plays a dominant role for the aerosol concentration lofted by CP2.

ACKNOWLEDGEMENTS

I have been incredibly fortunate so far along my science journey to the completion of this thesis. First and foremost, I must thank my advisor, Dr. Susan van den Heever, and my co advisor Dr. Leah Grant. I am grateful for their incredible mentorship, guidance, and they have helped me to grow as a scientist and do the best work that I can. I would also like to thank all the faculty at the CSU Department of Atmospheric for teaching great classes and for sharing their expertise. I would like to thank the staff for their patience and their kindness, their efforts have been extremely helpful through this process. I would like to thank Dr. Sonia Kreidenweis and Dr. Karan Venayagamoorthy for their time and generosity to serve on my master's committee. I am grateful for the contributions of van den Heever group members past and present: Kristen Van Valkenburg, Dr. Yasutaka Murakami, Dr. Alex Solokowsky, Dr. Sean Freeman, Dr. Bowen Pan, Dr. Ross Heikes, Ben Ascher, Bee Leung, Dr. Peter Marinescu, Dr. Jennie Bukowski, Katy Burger, Dr. Emily Riley Dellaripa, Dr. Brenda Dolan, Dr. I.T. Singh, Dr. Rick Schulte, Charles Davis, Rachel Auth, Nick Falk. Your feedback has improved this work and you have all been so kind and welcoming.

I am also grateful to have participated in two excellent field campaigns– the BACS-I and BACS-II campaigns–of which this study would have not been possible without. A special thank you to Dr. Leah Grant for her excellence in leading BACS-I and BACS-II. Thank you also to the BACS-I and BACS-II drones and sondes teams– Dr. Sean Freeman, Bee Leung, Nick Falk, Ben Ascher, Charles Davis, Jacob Escobedo, Allie Mazurek, Daniel Veloso-Águila, Tyler Barbero, Bryan Heffernan, Dr. Marina Nieto-Caballero, Lexi Sherman– for the great companionship that made BACS-I and BACS-II such a successful and fun campaign to be a part of.

Thank you to the wonderful mentors during my time as an undergraduate who helped me explore my interests and opened many doors for me, especially Dr. Joel Thornton, and Lexie Goldberger who helped prepare me for graduate school.

Thank you to my friends from Fort Collins and far for their encouragement and great company. Thank you also to my family for their endless support. I must especially thank my husband Ryan for your constant support and for always trying new things with me, including moving across the country.

I would lastly like to acknowledge funding from NSF grants #AGS-2105938 and #AGS-2029611 and thank them for their generosity in supporting this thesis.

TABLE OF CONTENTS

Chapter 1: Introduction

1.1 Cold Pools and Density Currents

Cool negatively buoyant air that forms from evaporation of the rain produced by a thunderstorm, known as a cold pool, sinks and then spreads laterally as a density current at the surface (Benjamin 1968; Droegemeier and Wilhelmson 1985a). Density currents form when there are differences in densities between two fluids. Early theoretical and laboratory tank experiments explored the structure and dynamics of density currents and found that they have a distinct head (Benjamin 1968) with a "lobe and cleft" structure (Simpson 1969), as well as their own internal flow (Middleton 1966). Additional tank studies found that density currents undergo dissipation by wave breaking (Keulegan 1958) and ambient turbulence (Linden and Simpson 1986).

The propagation of a density current has been found to relate to the properties of the fluid it is travelling through by the Froude number (e.g., Benjamin et al. 1968, Von Kármán 1940). The Froude number of a density current is calculated by:

$$\mathrm{Fr} = \frac{\mathrm{U}}{\sqrt{\mathrm{g'h}}} \tag{1}$$

where U is the rate of advance by the density current, g' is the rate of the reduced gravity in the density current, and h is the height of the density current. Theoretically, the Froude number has two limits for gravity currents through the relationship $\phi = h/H$ where H is the depth of the channel the density current is propagating through. Froude numbers similar to those of density currents have been observed in the atmosphere, implying that some atmospheric phenomena behave like density currents.

Cold pools in the atmosphere were first described as gusty thunderstorm outflows in the Thunderstorm Project by Byers and Braham (1949) over 70 years ago. However, it was a few decades before the dynamics and characteristics of observed cold pools were found to be similar to laboratory and theoretical density currents. While early theoretical and laboratory work revealed key processes and characteristics of density currents, atmospheric convection has a Reynolds number several order of magnitudes greater than that in a tank (Simpson 1997), which indicates that atmospheric cold pools are difficult to accurately model in a tank. In one of the earliest numerical modeling studies of cold pools, Droegemeier and Wilhelmson (1987) found that a grid spacing of 100 m or finer is required to properly simulate Kelvin Helmholtz waves, which act to dissipate cold pools. Recent studies have simulated cold pools using Large Eddy Resolving (LES) models to represent turbulence, entrainment, boundary layer turbulence, and land surface interactions and have found them to be crucial to the evolution of cold pools (e.g., Böing et al. 2012; Bukowski and van den Heever 2022; Grant and van den Heever 2016, 2018; Gentine et al. 2016; Kurowski et al. 2018). Thus, to study cold pools accurately, the roles of small-scale features such as turbulent entrainment and land surface interactions must be considered.

1.2 Cold Pool Interactions with Convection

Cold pools have been found to be a critical component of convective storms. One of the ways cold pools influence convective storm properties is through their impact on storm lifetime and intensity. Going back to the first observations of cold pools, Byers and Braham (1949) noted how cold pools cut off the flow of warm moist air into updrafts, which resulted in faster dissipation of convective storms. This impact of cold pools was later investigated and verified in

a modeling study by Droegemeier and Wilhelmson (1985a). However, cold pools can also lengthen the lifetime of a convective storm and help to intensify it. For instance, Houston and Wilhelmson (2011) found that cold pools act to deepen the ascent into quasi-linear storm updrafts in a low shear environment, which promoted a longer storm lifetime compared to isolated storms with weaker, shallower cold pools. Additionally, cold pools have been found to help with the transition between shallow and deep convection by reducing the lateral entrainment of environmental air (e.g., Böing et al. 2012; Khairoutdinov and Randall 2006; Kurowski et al. 2018).

Cold pools also play a crucial role in storm organization and propagation speeds. A classic theory, known as RKW theory (Rotunno et al. 1988; Weisman and Rotunno 2004), found that cold pools are critical for maintaining the organization and intensity of squall lines. RKW theory states that environmental vorticity generated by low-mid level wind shear interacts with the vorticity generated by the cold pool head, which itself is controlled by the intensity and depth of the cold pool. If the two vorticities are balanced, the squall line will have an optimally "upright" updraft, which helps organize the squall line and intensify it. If the two vorticities are not balanced, the updraft is tilted, which acts to weaken the squall line compared to if the vorticities were balanced. While RKW theory has some limitations, it has been successfully applied to observations and modeling studies of squall lines in the midlatitudes (e.g., Bryan et al. 2004, 2006). Contrastingly, Grant et al. (2018) found that the propagation and organization of mesoscale convective storms in a tropical oceanic regime were influenced more by gravity waves than cold pools.

While cold pools are important for the properties of preexisting convective storms, particularly in the midlatitudes, they also play a crucial role in generating new convection. Cold

pools can initiate storms through mechanical forcing (Droegemeier and Wilhelmson 1985a,b; Purdom 1976; Meyer and Haerter 2020), thermodynamic forcing (Feng et al. 2015; Langhans and Romps 2015; Tompkins 2001; Torri et al. 2015; Schlemmer and Hohenegger 2016), and cold pool collisions (Droegemeier and Wilhelmson 1985a,b; Falk and van den Heever 2023; Purdom 1982; Wilson and Schreiber 1986). Mechanical forcing refers to a parcel of air being physically lifted to its LFC by the circulation at the leading edges of cold pools (e.g., Droegemeier and Wilhelmson 1985a,b; Purdom 1976; Meyer and Haerter 2020; Moncrieff and Liu 1999). Thermodynamic forcing, on the other hand, refers to convection initiated by a change in the moisture and temperature profile inside the leading edges of cold pools, which acts to lower the thermodynamic energy barrier for convective initiation by lowering the level of free convection (Feng et al. 2015; Langhans and Romps 2015; Tompkins 2001). Finally, when cold pools collide, they "squeeze out" the air between them, which results in a strong updraft that can lift parcels to their LFC or initiate convection through changes in the thermodynamic profile as a result of the collision (Droegemeier and Wilhelmson 1985a,b; Falk and van den Heever 2023). In the midlatitude environment of Colorado, Wilson and Schreiber (1986) found that 79% of storms were initiated by convergent lines, which were mostly found in association with cold pools. In the moist tropical regime of the Amazon, cold pools and cold pool collisions were also identified to initiate new convective storms in 52% of over 300 storms observed (Lima and Wilson 2008).

Cold pool collisions have been a focus of several previous studies. For instance, Intrieri et al. (1990) found that in Colorado when a warmer cold pool collided with a colder cold pool, the warmer air was lifted over the colder air and that when cold pools collided, they were larger, more negatively buoyant, and moistened the environment more than isolated cold pools. In a tropical maritime environment, Torri and Kuang (2019) found that cold pools tend to cluster and

collide 10 minutes within forming. Additionally, Meyer and Haerter (2020) found that more total updraft mass flux was created due to cold pool collisions compared to an isolated cold pool using idealized simulations. Falk and van den Heever (2022) simulated cold pool collisions in continental and maritime environments, and found that mechanical and thermodynamic forcing of new convection by cold pool collisions were most sensitive to the initial temperature deficit of the cold pools. They also noted that mechanical forcing tends to peak for colliding cold pools starting at an optimal initial separation distance as a result of the balance between the creation and dissipation of kinetic energy, and that the optimal initial distance for the peak thermodynamic forcing is greater than that for mechanical forcing.

The new convection generated by cold pools – either through collisions with other cold pools or by mechanical or thermodynamic forcing – may produce another cold pool. This new cold pool may propagate through the same location as the original cold pool that initiated the new convection. Cold pools passing through the same location, in the same day during daylight hours, will be referred to as "cold pool trains" throughout this study. Cold pools propagating through the same location have seldom been studied, if at all, and represent a different way that cold pools may interact without colliding. Cold pools in a cold pool train may affect the ability of the next cold pool in the train to propagate and to lift air by virtue of influencing the atmospheric environment ahead of the next cold pool.

1.3 Cold Pool Implications for Aerosols

In addition to affecting storms directly through the maintenance and initiation of convective storms, cold pools can transport and loft aerosols, such as dust (Bukowski and van den Heever 2022; Knippertz et al. 2009a; Seigel and van den Heever 2012; Miller et al. 2008,

2019). Strong cold pool winds can loft large amounts of dust and form haboobs. The amount of dust lofted by haboobs is substantial and can linger for a long time in the atmosphere (Bukowski and van den Heever 2021; Flamant et al. 2007; Miller et al. 2008, 2019; Roberts and Knippertz 2014). Haboob dust lofting has been found to be sensitive to land surface type and the properties of the initial cold pool relative to the environment (Bukowski and van den Heever 2022). Dust in the atmosphere can have significant implications for storms. For instance, dust can act as cloud condensation nuclei (Twohy et al. 2009) and ice nucleating particles (e.g., DeMott et al. 2003; Field et al. 2006; Prenni et al. 2007; Twohy and Poellot 2005; Twohy et al. 2017). Dust lofted by haboobs can also be ingested by storms (Seigel and van den Heever 2012), which may influence convective lifetime and precipitation amounts. In addition to having impacts on storms, dust lofted by haboobs has implications for human health (Goudie 2014; Middleton 2017), affects Earth's radiative budget (e.g., Slingo et al. 2006; Sokolik and Toon 1996), and decreases visibility to hazardous conditions (Baddock et al. 2013; Middleton 2017). Additionally, dust lofted by haboobs can account for a fraction of the total dust sources for some regions to well over half the amount in other regions (Bou Karam et al. 2009).

While the majority of previous literature has focused on dust lofting by haboobs, cold pools can also transport and loft other types of aerosols. For example, increases in bioaerosol concentrations have been linked to cold pool passages (e.g., Emmerson et al. 2021; Hughes et al. 2020; Marks et al. 2001). Bioaerosols may be important to convective storm properties. Intact pollen grains can rupture into hundreds of submicron particles, often referred to as sub pollen particles (SPPs) (Grote et al. 2001, 2003). Pollen rupture into SPP has been theorized to be caused by increased humidity, precipitation, lightning and increased wind speeds associated with convective storms (Emmerson et al. 2021; Grote et al. 2001, 2003; Hughes et al. 2020; Miguel et

al. 2006; Newson et al. 1997; Stone et al. 2021; Subba et al. 2021, 2023; Wozniak et al. 2018). Both pollen and their SPPs can act as cloud condensation nuclei (CCN) (Steiner et al. 2015; Wozniak et al. 2018) and SPPs in particular can be effective warm temperature ice nucleating particles (INPs) (Gute and Abbatt 2018; Pummer et al. 2012; Dreischmeier et al. 2017; Burkart et al. 2021; Diehl et al. 2001; Werchner et al. 2022; Murray et al. 2012).

Bioaerosols can also pose a risk to human health. The increase in bioaerosol concentrations following the passage of convective storms and their associated cold pools, including pollen and their SPPs, have been linked to a phenomenon referred to in the literature as "thunderstorm asthma" (Bannister et al. 2020; Beggs 2017; D'Amato et al. 2019; Emmerson et al. 2021; Marks et al. 2001; Newson et al. 1997; Taylor and Jonsson 2004; Thien et al. 2018). Thunderstorm asthma refers to a sharp increase in asthma hospitalizations following the increase of bioaerosols after the passage of a convective storm and its cold pool. Most of the previous literature has investigated the factors important for increased hospitalizations and pollen emissions, but few, if any, studies have investigated how cold pools vertically and horizontally distribute bioaerosols. Marks et al. (2001) hypothesized that after the pollen is released from plants following rainfall, that cold pools transport the pollen to their edges. Since the study by Marks et al. (2001), there have been different methods proposed describing how the pollen is released (Burkart et al. 2021; Emmerson et al. 2021; Grote et al. 2001, 2003; Hughes et al. 2020; Miguel et al. 2006; Stone et al. 2021; Subba et al. 2021, 2023; Werchner et al. 2022; Wozniak et al. 2018; Zhang et al. 2014), but no studies have been conducted on how the pollen is transported within the cold pool. Bannister er al. (2020) found that convergence lines, which included cold pools, were a critical component of thunderstorm asthma, but were not sufficient to explain the increased hospitalizations. Therefore, there is a need for investigations into how cold pools

transport bioaerosols vertically and horizontally. Additionally, pollen and other bioaerosols that are emitted after a convective storm and cold pool passage may be further redistributed by a cold pool that passes over the same location later in the same day. Cold pools may transport and loft bioaerosols, and also other types of aerosols, differently in magnitude and direction depending on whether the cold pool came before or after another cold pool.

1.4 Thesis Outline and Objectives

In Chapter 2, we investigate how the dynamics of cold pools in cold pool trains vary, how the different cold pools in the trains may affect the horizontal and vertical distributions of aerosols, and how these results may change if the properties of the subsequent cold pool change. We hypothesize that the first cold pool in the cold pool train will loft the greatest concentration of aerosol compared to the subsequent cold pool, and that these differences are due to changes in the environment ahead of the subsequent cold pools, either from the passage of the first cold pool or by other processes such as radiative or land surface processes. Through the analysis of passive tracers to represent aerosols in idealized simulations of two cold pools, we find that there are large differences between the concentrations of aerosols lofted by the cold pools in the cold pool train, and that these differences are driven by the stabilization and the increased wind shear in the environment as a result of the leading cold pool passage. A manuscript that is being prepared for submission to the *Journal of the Atmospheric Sciences* (Neumaier et al. 2023, *in prep*)[1] comprises Chapter 2. Finally, in Chapter 3, we describe the conclusions and implications of this study.

[1] This study, called "Cold Pool Train Dynamics and Transport" co-authored by L.D. Grant, S.C. van den Heever, B.D. Ascher, J. Escobedo, N.M. Falk, S.W. Freeman, G.R. Leung, A.C. Mazurek, D.S. Veloso-Aguila, P.J. DeMott, S.M. Kreidenweis, R.J. Perkins, and E.A. Stone is being prepared for submission to the *Journal of the Atmospheric Sciences.*

Chapter 2: Cold Pool Train Dynamics and Lofting

2.1 Introduction

When precipitation from a convective storm evaporates, a region of negatively buoyant cold air, called a cold pool, forms and sinks to the surface, subsequently spreading out laterally along the surface as a density current (Benjamin 1968; Droegemeier and Wilhelmson 1985a). Cold pools have implications for weather, climate, and air quality (e.g., Fujita 1978; Garcia-Carreras et al. 2013; Miller et al. 2008). For instance, cold pools can affect a storm's intensity, lifetime, and organization (Weaver and Nelson 1982; Rotunno et al. 1988; Weisman and Rotunno 2004). Cold pools can also initiate new storms, mechanically through the lifting of air at their leading edges (Purdom 1976; Weaver and Nelson 1982), thermodynamically by changing the temperature and moisture profiles along their leading edges (Tompkins 2001), or through collisions with other cold pools (Droegemeier and Wilhelmson 1985a,b; Falk and van den Heever 2023).Wilson and Schreiber (1986) found that 79% of storms over the midlatitude environment of Colorado were initiated by convergent lines, often associated with cold pools. Additionally, Lima and Wilson (2008) noted that out of over 300 storms observed in the Amazon - a moist tropical regime - the most common initiation mechanism was identified to be convective outflows. The new convection initiated by cold pools may then also produce other cold pools. These cold pools often then pass over the same location as the previous cold pool. However, there have been few, if any, studies examining how the properties and behavior of two cold pools passing over the same location on the same day may vary. In this study, we will refer to cold pools passing over the same location in the same day during daylight hours, *without colliding*, as a "cold pool train". Each cold pool in a cold pool train may influence the

atmospheric environment and land surface ahead of the next cold pool in the train, thereby influencing the following cold pool's propagation speed as well as its ability to loft air.

In addition to lifting air along and over their leading edges, cold pools may loft aerosols, such as dust (Bukowski and van den Heever 2022; Knippertz et al. 2009a; Seigel and van den Heever 2012a; Miller et al. 2008, 2019). Haboobs are formed when strong cold pool winds loft large amounts of dust from the surface, and dust within haboobs is often relatively long lived in the atmosphere (Bukowski and van den Heever 2021; Flamant et al. 2007; Miller et al. 2008; Roberts and Knippertz 2014). Haboob dust lofting can account for as much as 60% of dust sources in some regions, although less than 10% in others (Bou Karam et al. 2009). Dust can affect Earth's radiative budget (e.g., Slingo et al. 2006; Sokolik and Toon 1996), threaten respiratory health (Goudie 2014; Middleton 2017), and act as both cloud condensation nuclei (Twohy et al. 2009) and ice nucleating particles (e.g., DeMott et al. 2003; Field et al. 2006; Prenni et al. 2007; Twohy and Poellot 2005; Twohy et al. 2017). Previous literature has found that lofted cold pool dust can also be ingested into storms (Seigel and van den Heever 2012a), which may influence storm lifetimes and precipitation amounts. Bukowski and van den Heever (2022) demonstrated that haboob dust lofting is sensitive to land surface type and the maximum temperature perturbation relative to the pre cold pool air.

While most previous literature has focused on cold pool *dust* lofting, other types of aerosols can also be lofted by cold pools. For instance, several studies have linked an increase in bioaerosols to convective cold pool passages (e.g., Emmerson et al. 2021; Hughes et al. 2020; Marks et al. 2001). Bioaerosols in the atmosphere have important implications for both weather and human health. Under certain conditions, pollen, a type of bioaerosol, can rupture into SPPs that can be particularly effective warm-temperature INPs (Gute and Abbatt 2018; Pummer et al.

2012; Dreischmeier et al. 2017; Burkart et al. 2021; Diehl et al. 2001; Werchner et al. 2022; Murray et al. 2012). Pollen and their SPP can also act as CCN (Steiner et al. 2015; Wozniak et al. 2018). Pollen and other bioaerosols have been linked to a phenomenon referred to as "thunderstorm asthma" where a sharp increase in asthma hospitalizations follow the passage of convective storms and their cold pools (Bannister et al. 2020; Beggs 2017; D'Amato et al. 2019; Emmerson et al. 2021; Marks et al. 2001; Newson et al. 1997; Taylor and Jonsson 2004; Thien et al. 2018). The emission and rupture of pollen is believed to be linked to increased humidity, precipitation, lightning, and increased wind speeds associated with convective storms (Emmerson et al. 2021; Grote et al. 2001, 2003; Hughes et al. 2020; Miguel et al. 2006; Newson et al. 1997; Stone et al. 2021; Subba et al. 2021, 2023; Wozniak et al. 2018). While much of the literature around thunderstorm asthma has attempted to disentangle the meteorological factors important for pollen emission and rupture, there are few, if any, studies on the role of cold pools in vertically and horizontally distributing bioaerosols. Marks et al. (2001) hypothesized that cold pools transport the pollen that is released by the rainfall responsible for forming the cold pool, and the release of pollen responsible for thunderstorm asthma has been proposed to occur via different methods (Burkart et al. 2021; Emmerson et al. 2021; Grote et al. 2001, 2003; Hughes et al. 2020; Miguel et al. 2006; Stone et al. 2021; Subba et al. 2021, 2023; Werchner et al. 2022; Wozniak et al. 2018; Zhang et al. 2014). Bannister et al (2020) investigated the influence of convergence lines, including cold pools, on thunderstorm asthma attacks and found that while convergence lines were a crucial component, they were not sufficient to produce a thunderstorm asthma epidemic. Thus, there is a need for studies investigating the role of cold pools in transporting and distributing bioaerosols. Additionally, pollen emissions after the passage of a cold pool may be transported and lofted by subsequent cold pools passing over the same

location. It is unknown whether the subsequent cold pools in a cold pool train may loft bioaerosols in the same way as the leading cold pool, or whether such lofting is different, both in magnitude and direction. Given the impacts of cold pools on their atmospheric and land surface environments, the lofting by the trailing cold pools in the train may be quite different.

During the BioAerosol and Convective Storms (BACS) Phase I (BACS-I) field campaign (see 2.2a for a more detailed description of the BACS field campaign), we observed multiple cases of cold pool trains. As demonstrated above, the dynamical behavior, lofting, and transport of aerosols by cold pool trains has not been studied previously. Thus, in this study we ask: *How do the dynamics of cold pools in "cold pool trains" vary, how do they affect the vertical distribution of aerosols, and how do the results change if the properties of the subsequent cold pool change?* We hypothesize that the first cold pool in the train lofts the highest concentration of aerosol compared with the subsequent cold pool(s), and that these differences are driven by changes to the environment due to the passage of the first cold pool and / or other radiative, land surface, or atmospheric processes. To address this question, we use idealized simulations of cold pool trains motivated by a case observed during BACS-I. Through the analysis of passive tracers in these simulations, we show that there are substantial differences between the concentration of tracers lofted by the cold pools in the cold pool train, assess the physical processes explaining such differences, and discuss the implications of the transport of aerosols by cold pool trains for the ingestion of aerosols into convective storms.

2.2 Methods

a. BACS-I description and case selection

BACS-I aimed to investigate the feedbacks between bioaerosols and convective storms, including how bioaerosol concentrations are influenced by cold pool passages. BACS-I was conducted in May and June 2022 in Nunn, Colorado at the National Science Foundation (NSF) National Ecological Observing Network (NEON) site in the Central Plains Experimental Range (CPER) (Figure 2.1a). BACS-II followed BACS-I, and was held in May and June 2023. May-June was chosen because those months are climatologically the most convectively active for the Northern Colorado and southern Wyoming regions and also overlap with tree and grass pollen season. CPER is a semi-arid short grass plains site and is representative of the grasslands across the central US plains. In addition, CPER is surrounded by 3 topographical features where convection often initiates (Figure 2.1a), so cold pools at the site are likely to come from all directions and thus is an ideal location to observe cold pools. Dynamic and thermodynamic measurements were taken using radiosondes, small uncrewed arial vehicles that flew up to 350 meters above ground, and a surface meteorological station.

Fourteen intensive operation periods (IOPs) comprised BACS-I, during which 26 cold pools were measured. On 7 of 14 IOPs, cold pool trains were observed, two of which are shown in Figures 2.1c and 2.1d. During the first case study that occurred on 6 June 2022, a cold pool train passed CPER (Figure 2.1d) that was formed by scattered and multicell storm systems. The first cold pool of the train had a temperature deficit of ~1 K (Figure 2.1d, 1330 MT), the second a temperature deficit of 1K (Figure 2.1d, 1530 MT), and the third a temperature deficit around 5 K (Figure 2.1d, 1630 MT), compared to the temperatures observed before each of their passages.

Thus, the cold pools in this cold pool train were observed to be either stronger or weaker than the previous cold pool in the train.

During the second case study on 29 May 2022, two squall lines and their associated cold pools passed CPER. The first cold pool's gust front that passed represented a merger between cold pools to the northwest and southwest of the CPER, and it was visible by a thin arc of reflectivity from the radar (region "A" in Figure 2.1b). The maximum surface temperature deficit associated with its passage was ~10 K relative to the temperature just before its passage (Figure 2.1c), and it was the most intense cold pool observed during BACS-I. The second squall line is marked "B" in Figure 2.1b and its cold pool passed CPER ~1.5 hours after the first cold pool passage. The second cold pool was weaker than the first; it had a temperature deficit of ~1 K at the surface (Figure 2.1c). We chose this case as the motivation for our modeling simulations to examine the impacts of a first intense cold pool on the properties and behavior of a second cold pool, and to determine whether there may be significant differences in their impacts on aerosol transport and redistribution.

b. Idealized model and Control experiment set up

A suite of idealized simulations are conducted using the Regional Atmospheric Modeling System (RAMS) version 6.3.02 (Cotton et al. 2003; Saleeby and van den Heever 2013; van den Heever et al. 2022). We use idealized simulations to investigate directly how cold pools in cold pool trains distribute aerosols. The details of the model set up are listed in Table 2.1. We use a horizontal grid spacing of 100 meters and a vertical grid spacing of 50 meters through the lowest 4 km (Table 2.1) in order to appropriately represent the turbulent cold pool processes (Bryan et al. 2003; Falk and van den Heever 2023; Grant and van den Heever 2016; Hirt et al. 2020;

Knippertz et al. 2009b; van den Heever et al. 2021). The meridional and zonal lateral boundaries are cyclic. Through the upper 800 m of the model, there is a Rayleigh dampening layer applied with a 60 second timescale to prevent the reflection of waves off the model top.

The atmospheric model is coupled with the Land Ecosystem-Atmosphere Feedback version 3 surface model (Walko et al. 2000), where the vegetation and soil properties interact dynamically with the atmosphere through surface fluxes. We initialize the domain with short grass vegetation and sandy clay loam soil classes to represent the observed surface conditions at CPER and hence mid-latitude dry continental environments. Similar to Grant and van den Heever (2018) and Falk and van den Heever (2023), water vapor is not allowed to condense in these idealized simulations in order to exclude the additional complexities brought about aerosol-precipitation-cold pool feedbacks. As this is the first study of cold pool trains and the role they play in aerosol lofting, it is important to be able to identify the predominant processes at play, before assessing the role of such feedbacks.

For the CONTROL experiment, we initialize the model horizontally homogeneously at 1800 UTC (noon local time) using a smoothed environmental sounding from BACS-I IOP03 (Figure 2.2a). We then integrate the model for two hours to allow the boundary layer and surface fluxes to develop (Figure 2.2c(i)). After two hours, we then initialize a single cold bubble, the details of which are provided below, and integrate the model forward in time, thereby allowing the cold bubble to drop and spread out laterally upon reaching the surface (Figure 2.2c(ii)). Two hours after the initialization of the first cold bubble, we release another cold bubble with the same properties and location as the first bubble. As the first cold bubble has moved out laterally, the second cold bubble is released into the environment modified by the first cold pool (Figures 2.2b and 2.2c(iii)). The simulation is once again integrated forward in time for an additional two

hours to allow the second cold bubble to propagate outwards (Figure 2.2c(iv)). A separation time of two hours was chosen to represent the maximum time we observed between two cold pools passing through the site during BACS-I. Since microphysical processes are excluded in these simulations, the cold pool is not continuously fed by rainfall evaporation, and the simulated cold bubbles are therefore representative of transient, dissipating cold pools. Although the cold pools produced in IOP03 were generated and fed by squall lines, we also observed several cases of dissipating cold pools that were several 10s of kilometers away from their parent storms.

The two cold bubbles in the CONTROL experiment were initiated about 50 km south of the domain center with a cosine squared function that is coldest in the center and warms as the bubble extends in the z and y-directions. Across the x direction, the cold bubbles have the same temperature. The maximum temperature deficit of the cold bubbles relative to their environments they initiate in is 20 K so that by the time the cold bubble reaches the surface and begins to spread, its temperature deficit is representative of the first intense (10 K) cold pool we observed during IOP03. The cold bubbles are 30 km wide in the y-direction, and extends across the entire domain in the x-direction, so that a line cold pool, similar to that of the observed squall line cold pools, is produced. The initial cold bubbles are 3 km deep to replicate the deep cold pool we observed during IOP03. Throughout the rest of this study, the first cold pool will be referred to as cold pool 1 (CP1) and the second cold pool as cold pool 2 (CP2).

c. Sensitivity Experiments

While the temperature deficits of the two bubbles released in the CONTROL experiment are the same, we observed situations during BACS in which the cold pools comprising the cold pool trains had different temperature deficits from one another. More specifically, during IOP03,

a smaller temperature deficit was observed between the cold pool and its environment with the passage of the second cold pool in the train compared to the first, however, there were other cases during which second cold pool in the train had similar temperature deficits compared to the first cold pool in the train (e.g., Figure 2.1d). Furthermore, while the two squall line cold pools passed the CPER within ~90 minutes of each other (Figure 2.1c), on other days, cold pools passed between 30 and 120 minutes after a previous cold pool passage. In order to represent the variations in cold pool temperature deficits and time intervals, we conduct two suites of sensitivity experiments.

In the first suite of sensitivity experiments, we set the maximum temperature deficit of the second cold bubble to 5K and 10K (Table 2.2), while leaving all the other parameters of the second cold bubble the same. These sensitivity simulations are referred to as "MODERATE" (10K) and "WEAK" (5K). In the second suite of sensitivity tests, we initialize the second cold bubble 30, 60, and 90 minutes after the initialization of the first cold pool, with the same properties of the first cold bubble (Table 2.2). These sensitivity simulations are called "90MIN", "60MIN", and "30MIN". As we run each temperature and time interval variation both individually and simultaneously, this results in a total of 12 simulations, all of which are described in Table 2.2.

d. Passive Tracer Set-up

We make use of passive tracers in the simulations to assess how the cold pools loft and redistribute aerosols in a generalizable manner. While the tracers are advected and diffused, they are not microphysically active, do not interact with radiation, and have no mass. The different sets of tracers used in these experiments are tracked independently in RAMS, thereby allowing

us to identify and track the motions and transport of each set of tracers independent of the other tracers. The tracers in all of the sensitivity experiments are initialized in three steps:

Step 1: Background Tracers

The first set of tracers is initialized after the 2-hour boundary layer spin up. They are distributed horizontally homogeneously throughout the lowest 500 m AGL, but decrease exponentially with decreasing pressure throughout this 500 m depth (Figure 2.2d). These tracers are representative of aerosols emitted at the surface, such as dust and pollen, and will be referenced throughout this study as the "background tracer."

Step 2: Newly Emitted Tracers

Another set of tracers is released in the same location as the set of background tracers is initialized. These will be referenced throughout this study as the "newly emitted tracer." The newly emitted tracer is initialized with the same vertical and horizontal concentrations as the initial background tracer (Figure 2.2d), and is representative of aerosols emitted after the passage of CP1. Examples of aerosols emitted after the passage of CP1 include dust lofting by the first cold pool (Bukowski and van den Heever 2022; Knippertz et al. 2009a; Seigel and van den Heever 2012a) as well as pollen emissions (Emmerson et al. 2021; Grote et al. 2001, 2003; Miguel et al. 2006; Newson et al. 1997; Stone et al. 2021; Subba et al. 2021; Wozniak et al. 2018).

Step 3: Cold Pool and Environmental Tracers

Finally, two different sets of tracers in this study are initialized 10 minutes after the first cold bubble initialization and 10 minutes after the second cold bubble initialization in the CONTROL case only. One set of tracers is initialized within each of the two cold pools that develop in this case. The tracers are initialized 5 km behind both of the cold pool's downshear leading edge for 20 km within the cold pool (Figure 2.2e) for each cold pool, spanning the entire x-direction, where we define the leading edge as the location of the -2 K density potential temperature perturbation (Emanuel 1994) relative to the environment. The tracers are initialized with the same vertical profile as the initial profiles of the background and newly emitted tracers, and are horizontally homogeneous within their initial y bounds (Figure 2.2d and 2.2e). We will refer to these tracers as the "cold pool tracers". The other set of tracers is initialized 5 km ahead of the downshear leading edge of each cold pool in the CONTROL case throughout the rest of the domain (Figure 2.2e). These tracers have the same vertical profile as the other tracers and are similarly horizontally homogeneous within their initial y bounds (Figure 2.2d and 2.2e). We will refer to these tracers as the "environmental tracers". These two sets of tracers are used to distinguish between how the cold pool lofts environmental air compared to how the cold pool lofts its own air. We also tested initializing tracers throughout the entire vertical depth of the atmosphere, as well as initializing the tracer layers above 500 m AGL, but the results are qualitatively the same.

2.3 Results

a. Cold pool train evolution in CONTROL

Figure 2.3 demonstrates the evolution of the two cold pools in the Control case after the initial boundary layer spin up period as described in section 2.2. The shading in Figure 2.3 is the density potential temperature perturbation (Emmanuel 1994), which is defined as the perturbation from the environment ahead of the cold pool. The environmental density potential temperature is obtained by spatially averaging the density potential temperature over y=250 km to y=280 km. The initial location of the first bubble is shown in Figure 2.3a. In the first 15 minutes after initialization, the first cold bubble drops and spreads out upon reaching the surface. After 15 minutes, there are updrafts associated with both the left (upshear) and right (downshear) edges of CP1 (Figure 2.3b). The strongest surface winds are near the leading edge of CP1 (near y = 130 km in Figure 2.3b). As the cold pool spreads, it dissipates quickly due to Kelvin-Helmholtz wave breaking and strong surface sensible heat fluxes (Grant and van den Heever 2016, 2018; Knippertz et al. 2009b) associated with strong daytime heating. Since the cold pool is uniform in the x direction, the environmental air is located ahead of each cold pool in the y-direction and gets mixed into the cold pool, along with environmental air above the cold pool. The upshear side of CP1 (near y=80 km in Figure 2.3b) has winds that are opposite of the environmental profile, so that it propagates only very slowly throughout the cold pool evolution (Figure 3c-d). However, the downshear side of CP1 travels in the same direction as the background winds, so it moves ~70 km in one hour (Fig. 2.3a-d, near y = 190 km in 2.3d). As CP1 spreads and dissipates, the coldest air relative to the environment remains at ~y=120 km (Figure 2.3b-d). The wind speeds in and above the upshear side of CP1 decrease as the cold pool dissipates (Figure 2.3b-d).

After two hours, a second cold bubble with the same properties as the first (maximum temperature deficit of 20K relative to its environment; Figure 2.2c(iii)), 2.2b; Figure 2.3e) is initiated. For the first 15 minutes of the evolution of CP2 it drops and spreads to the surface similarly to CP1, but in doing so it merges with the remnants of CP1 (Figure 2.3e and 2.3f). The leading edges of CP2 are deeper than those of CP1 at 15 minutes after each cold pool's initialization time (compare Figures 2.3b and 2.3f), and there are also stronger updrafts associated with CP2's edges compared to CP1. The downshear leading edge of CP2 is about 1 km higher than CP1 for the entire 30-minute period after initialization (Figure 2.3 f-g). As CP2 evolves, it dissipates and spreads, though it propagates somewhat slower than CP1. One hour after CP2's initialization, the winds inside the cold pool are weaker compared to the winds after the first hour of CP1's evolution (compare Figure 2.3d and 2.3h). CP2's downshear leading edge travels ~55 km in one hour (Figure 2.3h, near y=175 km), which is slower than the propagation speed of CP1 which travels ~70 km in one hour. However, CP2's upshear edge travels ~the same distance as CP1's upshear edge for one hour after initialization (Figure 2.3d and 2.3h, near y = 75 km).

The passage of CP1 stratifies the environment as it propagates through it. Since CP1 mainly propagates downshear of its initial location, the stratified air remains mostly downshear and in the location of the second cold bubble initialization. This stratification decreases the environmental wind speeds ahead of CP2 through the lowest 1 km (Figure 2.3e). Therefore, the vertical wind shear from the surface to ~3 km is *greater* in CP2's initial environment compared to the environment that CP1 experiences (see wind profile comparisons in Figures 2.2a and 2.2b and winds in Figures 2.3a and 2.3e). Thus, CP2 experiences an environment that is more stable, has weaker background advecting winds, and has more low-level wind shear than the

environment that CP1 propagates through. Increased stability has been shown to *decrease* cold pool head height and increase its propagation speed (Liu and Moncrieff 2000; Seigel and van den Heever 2012b). However, due to the increased wind shear, especially for the downshear leading edge of CP2, the depth of CP2's head *increases*, which is consistent with previous work on the effects of wind shear on density currents (Xu and Moncrieff 1994; Liu and Moncrieff 1996; Bryan and Rotunno 2014), and thus wind shear has a dominant influence on the downshear leading cold pool edge height of CP2. CP2's slower propagation speed appears to be due to the weaker background advecting winds. Since CP1 did not propagate very far in the upshear direction, the wind and stability profile that CP2's upshear edge propagates into is only slightly modified compared to CP1's upshear environment. Thus, the upshear side of both cold pools propagates similarly, although CP2's upshear edge is a few hundred meters deeper compared to CP1's upshear edge.

b. Tracer Analysis

Figures 2.4 and 2.5 demonstrate how the first set of tracers evolve. The background tracer, initialized with the start of CP1, is shown with blue shading in Figures 2.4 and 2.5, while the newly emitted tracer that is initialized at the same time as CP2 is shaded purple. The tracer concentrations in Figures 2.4 and 2.5 are normalized by $1x10^{9}$ kg^{-1} since only the relative amounts are considered between the cold pools. Figure 2.5 is similar to Figure 2.4, except the vectors are cold pool relative winds in order to better highlight the flow within the cold pool and its environment. The cold pool propagation speed of each cold pool is subtracted off the horizontal wind component to calculate the cold pool relative winds. The propagation speeds of each cold pool are calculated by determining the distance travelled by the cold pool leading edge

every 5 minutes then taking the average speed from t=15 minutes to t=35 minutes after initialization. Fifteen minutes after the initialization of CP1, the background tracer outside of the cold pool mixes throughout the boundary layer, which is ~3.6 km deep, although the strongest concentration is still near the surface (Figure 2.4a and 2.5a). Inside the center of CP1, tracer concentrations are suppressed, because the relative flow within the cold pool transports the tracer toward the surface and toward the edges of the cold pool as the negatively buoyant air forces the airmass to sink and spread (Figure 2.4a and 2.5a). The updraft at the leading edge of CP1 lifts the tracer in and above the heads of the cold pool (Figures 2.4a and 2.5a). After thirty minutes, the highest tracer concentration is found at the downshear leading edge of CP1 (Figure 2.4b and 2.5b). There is also a local minimum of background tracer above the center of CP1 (Figure 2.5b, around y=125km and z = 1 km). The influence of the circulation at the downshear leading edge on the tracer distribution is seen in Figure 2.5b, where the updraft ahead of the leading edge of CP1 and the downdraft behind it coincide with the maximum tracer concentration.

Two hours after the initialization of CP1 and the background tracer, the newly emitted tracers are released at the same time as the initialization of CP2. After 15 minutes of cold pool evolution, on the upshear side of CP2, the newly emitted tracer mixes throughout the boundary layer, similarly to the background tracer (Figure 2.4d and 2.4g). Since CP1 did not propagate far in the upshear direction and mostly dissipated to the left of y=110 km after two hours (Figure 2.3e), the environmental air upshear of CP2 is similarly turbulent as the environmental air upshear of CP1. However, on the downshear side of each cold pool, the newly emitted tracer mixes less throughout the boundary layer compared to the background tracer, and thus there is a higher concentration of newly emitted tracer near the surface here compared to the background tracer (Figure 2.4g). The newly emitted tracer is less vertically mixed than the background tracer

on the downshear side of each cold pool because of the atmospheric stratification left by the passage of the first cold pool. Throughout the evolution of CP2, the concentration of the newly emitted tracer behind the downshear leading edge is more than double that of the background tracer concentration in the same location for CP1 (Figure 2.4g-i). Since less of the newly emitted tracer is being mixed throughout the depth of the boundary layer, there is more available for CP2 to loft over its leading edge (Figure 2.5c and 2.5d). As the downshear edge of CP2 is deeper, so the higher near-surface concentration of newly emitted tracer also gets lofted higher in the vertical (Figure 2.4h and 2.4i). Also, due to the fact that the newly emitted tracer mixes less in the boundary layer downshear of CP2, the tracer concentration inside the cold pool edge is much higher than the background concentration at similar altitudes above 500 meters (Figure 2.5c and 2.5d). The upshear edge of CP2 lofts a similar concentration of the newly emitted tracer compared to the concentration of background tracer lofted by the upshear edge of CP1 (Figure 2.4 g-i). The upshear edge of CP2 propagates similarly to the upshear leading edge of CP1; thus, it is unsurprising that these upshear cold pool leading edges loft a similar amount of tracer.

The background tracer also evolves with the initialization and evolution of CP2 and is shown in Figure 2.5e and 2.5f. After two hours of model integration, the tracers are mostly well mixed within the boundary layer, which is ~3.6 km deep, with the highest concentration of tracers located within the remnant CP1 (Figure 2.5e). The strong winds near the surface at the downshear leading edge of CP2 transport the background tracer ahead of the cold pool starting at 30 minutes after the second cold pool's initialization (Figure 2.5f near y = 150 km). Some of this tracer gets lofted after 35 minutes (not shown), but the concentration is only one-third of what is lofted by the first cold pool because it is already well mixed within the boundary layer when CP2

is initialized. At CP2's upshear edge, the background tracer lofted by the cold pool is indistinguishable from the background tracer concentration ahead of the cold pool (not shown).

The final set of tracers for the CONTROL experiment, the environmental and cold pool tracers as described in section 2.2, are initialized 10 minutes after the initialization of each cold pool in the train to distinguish between how cold pools loft their own air compared with the manner in which they loft distinct environmental air. After 5 minutes of environmental and cold pool tracer evolution, 15 minutes after the initialization of each cold pool, the environmental tracers start to mix within the boundary layer (Figure 2.6a and 2.6c, orange shading). The environmental tracer associated with CP2 does not mix as much compared to the CP1's environmental tracer because the turbulence downshear of CP2 is weaker compared to the well mixed boundary layer ahead of CP1 (compare Figure 2.6a and 2.6c), due to the CP1-induced stratification of the environment ahead of CP2. This is in agreement with the analysis and discussion of Figures 2.4 and 2.5. About 30 minutes after each cold pool's initialization, the environmental tracers are lifted by the downshear leading edge of each cold pool and transported above and behind the head of the cold pool (Figure 2.6b and 2.6d). The concentration of environmental tracer lofted by CP2 is more than double the concentration of environmental tracer lofted by CP1, again in keeping with the analysis and discussion of Figures 2.4 and 2.5. In CP1, the environmental tracer is lofted above and to the left of the downshear cold pool head, with only limited amounts of tracer being mixed into the head (Figure 2.6b, near y=155 km). However, while the environmental tracer is lofted above the head of CP2, there is a greater concentration lofted inside the cold pool head compared to that of CP1 (Figure 2.6d, near y =150 km). The environmental tracer ahead of CP2 is incorporated into the cold pool head because of the CP1-induced atmospheric stratification, while the environmental tracer ahead of CP1 mostly

stays outside of the cold pool boundary. The environmental tracer does not mix through CP1's boundary because the strong winds near the surface inside the head of CP1 act to push the tracer from its boundary.

Focusing our attention of the tracers released within the cold pools themselves (blue shading in Figure 2.6), it is evident that the cold pool tracers are stratified within the cold pools, and their concentrations are similar between the two cold pools (Figure 2.6a and 2.6c). Due to the cold pool air being negatively buoyant, the tracers are trapped near the surface within each cold pool in the train, particularly in the body of the cold pools (Figure 2.6a and 2.6c). The cold pool tracers in both cold pools are advected and hence spread out with the expanding cold pools, but they are not lifted by the leading edge (Figure 2.6b and 2.6d) being unable to do so due to the cold pools' negative buoyancy. In CP1, the cold pool tracer in the head does ultimately mix almost to the top of the cold pool, but does not mix outside the cold pool (Figure 2.6b, near y =155km). However, the cold pool tracer in CP2 only gets lofted to ~1.4 km (Figure 2.6d, near y = 150 km - though this is not evident in the figure due to the orange shading overlaying the blue shading), which is 1 km below its maximum height. Therefore, the cold pools struggle to loft their own air, which has also been shown in previous studies (Seigel and van den Heever 2012a). Thus, the high tracer concentrations in and around the cold pool head seen in Figures 2.4 and 2.5 come primarily from the air that the cold pools are propagating into, rather than from their own internal air, especially aloft.

c. Sensitivity Experiments

i. Cold pool strength sensitivity experiments

As described in section 2.2c, sensitivity experiments are conducted to test how changes in the second cold pool's strength and timing impact the dynamics and lofting mechanisms. Figure 2.7 shows the results of varying CP2's strength from 20K in the CONTROL simulation, to those with maximum temperature deficits of 10K (experiment "MODERATE) and 5K (experiment "WEAK"). Figure 2.7c and 2.7d demonstrate the cold pool structures 30 minutes after their initialization. Compared to CP2's structure in the CONTROL case after 30 minutes (Figure 2.7e), CP2 in the MODERATE case has a shallower head and propagates more slowly (Figure 2.7d, around y = 145 km). Additionally, the circulation around the cold pool head is weaker (Figure 2.7d). Since the temperature deficit is less than that in the CONTROL CP2 case, the MODERATE CP2 propagates slower (Benjamin 1968) and has weaker winds (Simpson 1969). For the WEAK CP2, it has already begun to dissipate 30 minutes after its initialization, as seen by the near surface dashed contour around y=140 km in Figure 2.7c. The remaining WEAK CP2 does not have a clear head circulation, and the deepest part of it is ~1km (Figure 2.7c, near y= 135 km), which is shallower than the heads of CP1 and CP2 in the CONTROL and MODERATE cases (compare Figure 2.7c and 2.7d to 2.7b and 2.7e).

The amounts of newly emitted and background tracer lofted by each cold pool in this suite of sensitivity tests are summarized in Figure 2.7a. This figure shows the vertical profiles of horizontally averaged tracer concentrations between 5 km to the right and 5 km to the left of the leading cold pool edge. For the background tracers (grey and dashed lines in Figure 2.7a), the highest concentration is lofted by CP1 (grey line in Figure 2.7a). Each CP2 in the temperature deficit strength tests have only slight differences in the concentrations of background tracer lofted by each of their downshear heads (dashed lines in Figure 2.7a), though the background tracer is lofted to higher altitudes with increasing temperature deficit of CP2, which is expected

given the different depths of the secondary cold pool heads (compare Figure 2.7c-2.7e). The background tracer is well mixed in the boundary layer after two hours of CP1's evolution (Figure 2.5e), so the differences in the strength of CP2 have little effect on the background tracer concentration aloft. Near the surface, the lofting of the newly emitted tracers by the MODERATE CP2 is the greatest, up until ~1.6 km AGL (the blue solid line in Figure 2.7a). Above 1.6 km AGL, the CONTROL CP2 is associated with the highest tracer concentration until ~3 km AGL (the black solid line in Figure 2.7a), above which CP1 in CONTROL has the highest concentration of lofted tracers (the grey line in Figure 2.7a). For CP2 in the MODERATE and WEAK cases, there is a greater amount of newly emitted tracer nearer the surface because of the limited capability of these weaker cold pools to loft them to greater heights due to their weaker updrafts and shallow heads compared to the CONTROL CP2 (compare Figure 2.7c and 2.7d to 2.7e). The CONTROL CP2 lofts ~twice as much newly emitted tracer as the CONTROL CP1 lofts background tracer through the lowest ~2.3 km AGL (Figure 2.7a), which agrees with discussion in the previous section. Above 3 km AGL, CP1 lofts the greatest tracer concentration (Figure 2.7a) due to the mixing of the background tracer throughout the boundary layer, which is ~3.6 km deep.

ii. Timing sensitivity experiments

Figures 2.8 and 2.9 describes the results of the CP2 timing sensitivity experiments, where the second cold bubble initialization time is varied between 30, 60, and 90 minutes, compared with the 2-hour time interval tested in the CONTROL simulation. Figure 2.8b-2.8e show the structure of CP2 30 minutes after their respective initialization times. Figure 2.9 shows a vertical profile of the mean horizontal wind speed between y=160 km and 180 km for CP1 and each CP2

in the timing sensitivity experiment at 30 minutes after their respective initialization times. CP2 in the 30MIN case (Figure 2.8b) is shallower and propagates faster than CP2 in the CONTROL case (Figure 2.8e). After only 30 minutes between the initialization of CP1 and CP2 in this experiment, the environment that CP2 is propagating into is the most stable out of any of the experiments because CP1 has dissipated the least (Figure 2.8b). The increased CP1-induced static stability leads to a shallower cold pool head. Previous literature has found that stable layers decrease the depth of a cold pool, which increases its propagation speed (Liu and Moncrieff 2000; Seigel and van den Heever 2012). Additionally, the horizontal wind shear in the 30MIN case organizes into two distinct layers: a layer of increasing horizontal wind speeds from the surface to 1.5 km AGL, and a layer with decreasing winds speeds from 1.5 km to 3 km AGL (Figure 2.8b and the light blue line in Figure 2.9). The 1.5 km level where the wind shear changes sign may also be limiting the second cold pool's height in the 30MIN case. As the time between cold pool initializations increases, the depth of the CP2 head increases until the 90MIN case, then decreases for the CONTROL case, and its propagation speed decreases (Figure 2.8b-e). There are three probable effects driving these changes in structure. First, as the time increases between cold pool initializations, CP1 spreads out further and dissipates. As the cold pool dissipates, the environment ahead of CP2 starts to destabilize due to surface sensible heat fluxes, generating a more turbulent boundary layer. This destabilization effect acts to decrease the second cold pool's propagation speed and increase its depth (Grant and van den Heever 2018; Liu and Moncrieff 2000; Seigel and van den Heever 2012b) Second, the increased turbulence also vertically mixes stronger winds aloft, thereby generally decreasing the vertical wind shear. All else equal, decreased vertical wind shear acts to reduce the cold pool depth, countering the destabilization impact on depth. Third, as CP1 dissipates, its average wind speed throughout its

depth decreases. This decreases the mean wind speed that CP2 propagates into (Figure 2.9) and therefore may be decreasing the overall propagation speed of CP2. Overall, the experiment with the greatest CP2 downshear head depth is the 90MIN case (Figure 2.8d), while the slowest propagating CP2 is the CONTROL experiment (Figure 2.8e) among the timing sensitivity experiments. This may be because CP2 in the 90MIN case has more wind shear in the 0-3km level ahead of the downshear leading edge than the same level for CP2 in the CONTROL case (compare Figure 2.8d and 2.8e and the navy and black lines in Figure 2.9). CP2 in the CONTROL case propagates the slowest apparently due to the fact that it has the weakest winds advecting it (Figure 2.9), and it is subjected to the least stable atmosphere of the timing sensitivity experiments.

Figure 2.8a summarizes the impact of varying the timing between cold pools in the cold pool train on tracer lofting for the newly emitted tracers and background tracers. Similarly to the temperature deficit sensitivity experiments, there are only small differences between the concentration of background tracer lofted by each CP2 (dashed lines in Figure 2.8a). Near the surface, the 30MIN case has the greatest newly emitted tracer concentration, followed by the 60MIN, 90MIN, and CONTROL cases (solid blue lines and black line in Figure 2.8a). The newly emitted tracers are trapped in the stable layer left behind by the first cold pool (Figures 2.8b-e), and as time between initializations increase, the increasing instability allows for the tracers to start mixing aloft more effectively thereby reducing near surface concentrations. However, above 500 m AGL, this trend reverses and the concentration of newly emitted tracers is greatest for the CONTROL case, followed by the 90MIN, 60MIN, and 30MIN cases (light blue, blue, and black lines in Figure 2.8a), being reflective of the time necessary to enhance the instability and to loft tracers to these heights. The tracer does not mix out of CP2 for the 30MIN

case; however, they do mix and loft above CP2 for the 60MIN, 90MIN, and CONTROL cases (Figure 2.8b-e).

Lastly, the results of all 12 sensitivity experiments, where the maximum temperature deficit and the time of the second cold pool initialization are varied both independently and simultaneously (see Table 2.2), are summarized in Figure 2.10. The newly emitted tracer concentrations lofted by CP2 in each experiment are first integrated up to 2.5 km AGL, approximately the height of the deepest cold pool head, and are then spatially averaged 5 km behind to 5 km ahead of the downshear leading edge, which is. The integrated values of the background tracer concentrations averaged over the same distance around the leading edge of CP1 are then subtracted from the integrated newly emitted tracer concentrations. In this way, the lofting by CP1 and CP2 can be compared fairly. Finally, the differences are integrated through 40 minutes (Figure 2.10a and 2.10c) and through 90 minutes (Figure 2.10b and 2.10d) of each cold pool's evolution to describe the total relative amount lofted by each cold pool. The cold pools in all simulations evolve for 40 minutes, but some entirely dissipate after 40 minutes, so 40 minutes was chosen as the first integration time. After 90 minutes, most of the other cold pools dissipate entirely, so 90 minutes represents the time over which total lofting can be compared among all the cold pools. The greatest concentrations of tracer lofted in the head of any of the cold pools occurs in the MODERATE (10K) cold pool after 40 minutes of evolution (blue circle in Figure 2.10a). Every CP2 except for the WEAK (5K) 30MIN case lofts more newly emitted tracer compared to the background tracer lofted by CP1 (Figure 2.10a-d). The WEAK 30MIN CP2 did not loft a large tracer concentration because this cold pool is shallow and has weak updrafts (not shown). After 40 minutes it is not clear whether timing between cold pools or temperature deficits impacts CP2 lofting the most (Figure 2.10a and 2.10c). However, it is clear that as the

cold pools are initialized farther apart in time, the temperature deficit of CP2 becomes more important for newly emitted tracer lofting, as evidenced by the larger spread among the temperature deficit tests for the CONTROL and 90MIN groupings than for the shorter timings (Figure 2.10c). Thus, as CP1 dissipates and the environment destabilizes, the amount of tracer able to be lofted becomes greater as the boundary layer mixes. After 90 minutes, there is more spread among the temperature deficit tests (Figure 2.10b than among the timing tests (Figure 2.10d), which implies the temperature deficit of CP2 has a greater impact than the timing separation between CP1 and CP2 on the amount of newly emitted tracer lofted by CP2's downshear leading edge for the lifetime of its evolution. The cold pools with lower temperature deficits dissipate faster, so it is unsurprising that after 90 minutes of each cold pool's evolution, the temperature deficit has a stronger impact than the timing separation between CP1 and CP2 on the amount of newly emitted tracer lofted by CP2.

2.4. Discussion

Figure 2.11 is a schematic of the cold pool train lofting mechanisms we have identified in our analysis of the idealized sensitivity experiments. Note that in this section we will refer to the tracers as aerosols. The cold pool motion in Figure 2.11 is to the right. The near surface background aerosol, represented by the black contours, rapidly mixes within the developing boundary layer. The first cold pool of the train (CP1) lofts these aerosols up and behind the cold pool head, with a maximum aerosol concentration occurring near the cold pool wake as a result. Within the cold pool itself, the background aerosol is advected towards the head of the cold pool by virtue of the cold pool circulations. As the first cold pool propagates outward, it stratifies the environment that second cold pool of the train (CP2) propagates into thereby reducing the

boundary layer mixing and weakening the winds near the surface. This increases the horizontal wind shear of the environment ahead of CP2 by more than 100%. Since the wind shear increases ahead of the second cold pool in the train, the leading-edge depth of CP2 increases due to the environmental negative vorticity that opposes the cold pool's positive vorticity at its leading edge (e.g. Liu and Moncrieff 1996; Rotunno et al. 1988; Xu 1992). At the same time, the propagation speed of CP2 decreases, which is probably due to the decrease in mean advecting wind speeds through the depth of CP2, which decreased as a result of CP1's dissipation. The increased static stability, which has been shown to decrease the depth of the cold pool head and increase propagation speed, competes against the effects of increased wind shear, which increases cold pool head depth (Xu and Moncrieff 1994; Liu and Moncrieff 1996, 2000; Bryan and Rotunno 2014; Seigel and van den Heever 2012). Since the CONTROL CP2 has a greater downshear leading edge depth than CP1 and is slower moving, changes to the mean wind speed and the wind shear appear to play a dominant role over stability in impacting the second cold pool's depth. However, the stabilization of the environment ahead (downshear) of CP2 also limits the amount of boundary layer turbulence. Thus, aerosols newly emitted after the passage of the first cold pool (represented by the brown contours in Figure 2.11), such as from the lofting of dust or from pollen emissions at the surface, have a higher concentration in the near surface atmospheric layers compared to the background aerosols ahead of CP1. CP2 then lofts these higher concentrations of near surface aerosol to a greater height than that of CP1 due to the increased depth of the CP2 head. This is supported by Figure 2.8a in which the concentrations of the newly emitted aerosol lofted by CP2 are more than double the concentration of background aerosol lofted by CP1. CP2 does loft the remaining background aerosols as well, but the concentrations

lofted are less than half of the background concentrations lofted by the first cold pool, as shown in Figure 2.7a.

The paragraph above describes the mechanisms seen in the CONTROL experiment. However, the cold pool intensities and timing between cold pools in cold pool trains were observed to vary in the BACS-I field campaign and so a suite of sensitivity tests are conducted by varying CP2's initial temperature deficit and timing relative to CP1. Changing the strength of CP2 changes the concentration of background aerosol lofted by CP2 by less than 1% throughout the cold pool head depth (dashed lines in Figure 2.7a), with the amount lofted increasing with increasing CP2 strength. However, the altitude to which the background aerosols are lofted varies with the CP2 strength, since the stronger secondary cold pools have deeper leading edges (as seen in Figure 2.7c-e). For the aerosols newly emitted after CP1, weaker CP2s loft smaller aerosol concentrations than stronger CP2s above ~1km AGL but have greater aerosol concentrations near the surface (solid lines in Figure 2.7a). The wind speed at the edge of the cold pool decreases in the weaker cold pools (Benjamin 1968, Simpson 1969), so the strength of the convergence between the cold pools' regions of positive vorticity and the environments' regions of negative vorticity decreases, leading to weaker updrafts ahead of the CP2s and shallower leading edges. Therefore, more of the newly emitted aerosol remains at the surface ahead of the CP2s compared to the CONTROL CP2, because less are lofted by the cold pool.

Additional sensitivity tests are conducted with the initialization of the second cold bubble 30, 60, and 90 minutes after initialization of the first cold bubble, in addition to the CONTROL case in which CP2 is initialized 2 hours after CP1. As the time interval increases between the cold pool initializations, the air ahead of CP2 becomes less stably stratified as CP1 increasingly dissipates due to radiative heating and sensible and latent surface fluxes. Thus, as the time

interval between the cold bubble initializations increases, the newly emitted aerosol mixes more effectively throughout the boundary layer as the near-surface atmosphere becomes less stratified. Additionally, the downshear leading edge head depth of CP2 generally increases until the 90MIN case, but decreases for the CONTROL case; and its propagation speed decreases as the time between cold bubble initializations increases (see Figure 2.8b-d). This is because the environment ahead of CP2 becomes increasingly less stable, the advecting winds through CP2's depth decrease, and the wind shear decreases as CP1 has more time to dissipate (e.g. Liu and Moncrieff 1996; Rotunno et al. 1988; Xu 1992, Xu and Moncrieff 1994; Liu and Moncrieff 1996, 2000; Bryan and Rotunno 2014; Seigel and van den Heever 2012). The amount of newly emitted aerosol lofted above ~1 km AGL therefore also increases as the time interval between cold pools increases. For the background aerosols, the results of the timing tests are similar to those from the temperature deficit experiments. The concentration of background aerosols lofted by each case in the sensitivity tests only varies by ~1%, but the greater the time between cold pool initializations, the higher aloft the background aerosols are transported (see dashed lines in Figure 2.8a) due to deeper downshear cold pool heads and greater mixing in the boundary layer.

Although only transient, linearly-oriented cold pools without any microphysics were simulated, the physical mechanisms and processes described here should be applicable to other cold pool and convective scenarios, though quantities may be variable. Storm updrafts and microphysical processes, for instance scavenging of aerosols by rain, could change the number of background and newly emitted aerosols available for the cold pools to loft. Additionally, aerosols can settle, especially large dust or intact pollen grains, which could impact the relative amounts lofted by the first and second cold pools.

2.5 Conclusions:

In this study, we investigate how the cold pools within cold pool trains – defined as cold pools passing through the same location on the same day during daylight hours, without colliding, - alter the distribution of aerosols. During the BACS-I field campaign, we observed several cases where multiple cold pools passed over the field site on the same day, which motivated this study. In one of these cases, two successive squall line cold pools were observed, which we have used as a guide for the numerical model experiments presented in this study. We ran Large Eddy Resolving simulations of two idealized, linearly-oriented cold pools that are initiated two hours apart. To emulate the lofting of aerosols, we use passive tracers to represent different aerosol scenarios: background aerosols, aerosols emitted after the passage of the first cold pool, within-cold pool aerosols, and environmental aerosols ahead of the cold pool which the cold pool propagates into. We also conduct sensitivity tests to examine the impacts of the maximum temperature deficit of the second cold pool and of its initiation time relative to that of the first cold pool. These sensitivity experiments represent the different scenarios of cold pool trains observed during BACS-I. This is the first study to numerically simulate cold pool trains and how they loft aerosols.

We find multiple physical processes that occur as a result of the first cold pool passage. The first cold pool (CP1) stably stratifies the environment downshear of the second cold pool (CP2), which, all else equal, acts to limit the depth of CP2's head and increases its propagation speed compared CP1. However, the stabilization of the environment ahead of CP1 increases the wind shear downshear of CP2 by decreasing the near surface horizontal wind speeds. This increased wind shear deepens the head of the cold pool, and the weaker near-surface winds decrease its propagation speed. These two effects have opposite impacts on cold pool head depth

and cold pool propagation speed (e.g. Liu and Moncrieff 1996; Rotunno et al. 1988; Xu 1992, Xu and Moncrieff 1994; Liu and Moncrieff 1996, 2000; Bryan and Rotunno 2014; Seigel and van den Heever 2012), however in this case, the changes to the wind profile have a stronger impact on the second cold pool's downshear head depth and propagation speed than the stability changes.

The temperature deficit sensitivity tests show that the CONTROL case, in which CP2 has a temperature deficit of 20K, has the deepest downshear head and fastest propagation speed, followed by the MODERATE, then WEAK second cold pools, with maximum temperature deficits of 10K and 5K, respectively. The timing sensitivity tests show the 90MIN CP2 has the deepest downshear head due to the greatest 0-3km horizontal wind shear and lowest environmental stability compared to the CP2s in the 30MIN and 60MIN cases, while the CONTROL CP2 propagated the slowest. The CONTROL CP2 may have propagated the slowest because it had the slowest mean advecting winds through the depth of CP2 and had lower stability than the other CP2s in the timing sensitivity experiments.

In examining the impacts of the CP1 and CP2 properties on lofting aerosols, we find that CP1 lofts the most background tracer at its leading downshear edge. CP2 in the CONTROL case lofts less than half of the background tracer than CP1, a result that is similar across all of the sensitivity tests. The tracer lofted by the cold pools' leading edges originate in the environment ahead of the cold pool, while the tracer originating in the cold pool remain trapped inside the cold pool. However, CP2 can loft a substantially greater concentration of tracer emitted *after* the passage of CP1, compared to CP1's lofting of the *background* tracer. These changes in lofting are driven by the stratification of the environment ahead of CP2 induced by CP1, which traps the newly emitted tracer near the surface thereby allowing for a greater concentration of tracer to be

lofted along CP2's leading edge, as opposed to being vertically mixed within the boundary layer. At the upshear edge of the cold pools, CP2 lofts a similar amount of newly emitted tracer as CP1 lofts of the background tracer because the tracers are similarly vertically mixed within the upshear environment.

The cold pool strength sensitivity tests show that the CONTROL CP2 lofts the most newly emitted tracer aloft, followed by the MODERATE, and lastly the WEAK CP2. The timing sensitivity tests show that the CONTROL CP2 lofts the most newly emitted tracer, followed by the 90MIN, 60MIN, and 30MIN cases. Overall, the temperature deficit of CP2 plays a more important role in tracer lofting than the timing between CP1 and CP2 through the lifetime of the cold pools, and the temperature deficit becomes relatively more important as the timing between cold pools increases. This has implications for potential transport and ingestion of aerosol into convective storms, where aerosols such as dust and biological particulates may serve as INP and CCN, subsequently affecting storm microphysics and dynamics. These results also highlight the need to include interactive aerosols, as well as the interactions and feedbacks between such aerosols and cold pool dynamics in forecast models, if aerosol distributions and their subsequent impacts on air quality and storm processes are to be accurately forecasted.

There are many future avenues of this research, including how different storm types and their associated cold pools may impact the aerosol lofting by the cold pools comprising cold pool trains, and to what extent the aerosols lofted by different cold pools in the train may be ingested into the parent or subsequent convective storms. Analysis of BACS-I and BACS-II data will also provide further insight into how the properties of cold pools in cold pool trains and their impacts on aerosol concentrations may vary, both at the surface and aloft, through the use of the thermodynamic and aerosol number concentration observations made using the small uncrewed

arial vehicles. Additionally, recent advances in other observation platforms, such as meteorological observing towers (e.g. Kirsch et al. 2021; Kruse et al. 2022; Sun et al. 2020), may provide more insight in the observed dynamics of cold pool trains and aerosol concentrations ahead and within cold pools in other environments. For example, Mai et al. (2023) analyzed observations of two colliding cold pools using a tower 365 m AGL, and Sun et al. (2020) used the same tower to collect vertically resolved black carbon data. Such observations can enhance our knowledge of the variability of cold pool properties and will also help to evaluate future case study simulations of cold pool trains in different environments.

2.6 Tables

Table 2.1: RAMS model idealized simulation settings common to all experiments.

Model	RAMS v6.3.02 (Cotton et al. 2003; Saleeby and van den Heever 2013; van den Heever et al. 2022)
Domain size (Y x X x Z)	300 x 25 x 13.35 km
dx, dy	100 m
dz	Constant 50 m up to 4 km, stretched with a stretching ratio of 1.02 up to a maximum of 200 m above 4 km
Timestep	0.75 s
Output frequency	5 min
Microphysics	Water vapor not allowed to condense
Turbulence	Smagorinsky (Smagorinsky 1963) with stability modifications by Lilly (1962) and Hill (1974)
Radiation	Harrington (Harrington 1997)
Surface model	LEAF-3 interactive (Walko et al. 2000)
Soil type	Sandy Clay Loam
Land surface type	Short Grass
Soil moisture	0.35 fraction of saturation for 11 vertical levels
Initialization time	1800 UTC
Initial environment	Environmental radiosonde from BACS-I IOP03
Coriolis	No
Freeslip	No
Boundaries	Lateral: Cyclic Top: Rayleigh dampening layer applied in the upper 800 m over a timescale of 60 s
1st Cold Bubble Initialization:	
Initialization time	2000 UTC
Maximum temperature deficit	20 K
Depth	Zmin = 25m, Zmax = 3025 m
Center	y = 105 km, z = 1525 m, uniform in x
Width	30 km in y
Type	cosine squared gaussian function

Table 2.2: Experiment names and settings for the secondary cold pool in the sensitivity experiments. Δt_1 is the time between cold pool 1 and 2 initializations (Figure 2.2c). ΔT_{max} is the maximum temperature deficit of the second cold pool (Figure 2.2c). The temperature deficit of the first cold pool is always 20K.

Experiment Name	ΔT_{max}	Δt_1
CONTROL	20 K	120 min
MODERATE	10 K	120 min
WEAK	5 K	120 min
90MIN	20 K	90 min
60MIN	20 K	60 min
30MIN	20 K	30 min
MODERATE 90MIN	10K	90 min
WEAK 90MIN	5 K	90 min
MODERATE 60MIN	10 K	60 min
WEAK 60MIN	5 K	60 min
MODERATE 30MIN	10 K	30 min
WEAK 30MIN	5 K	30 min

2.7 Figures

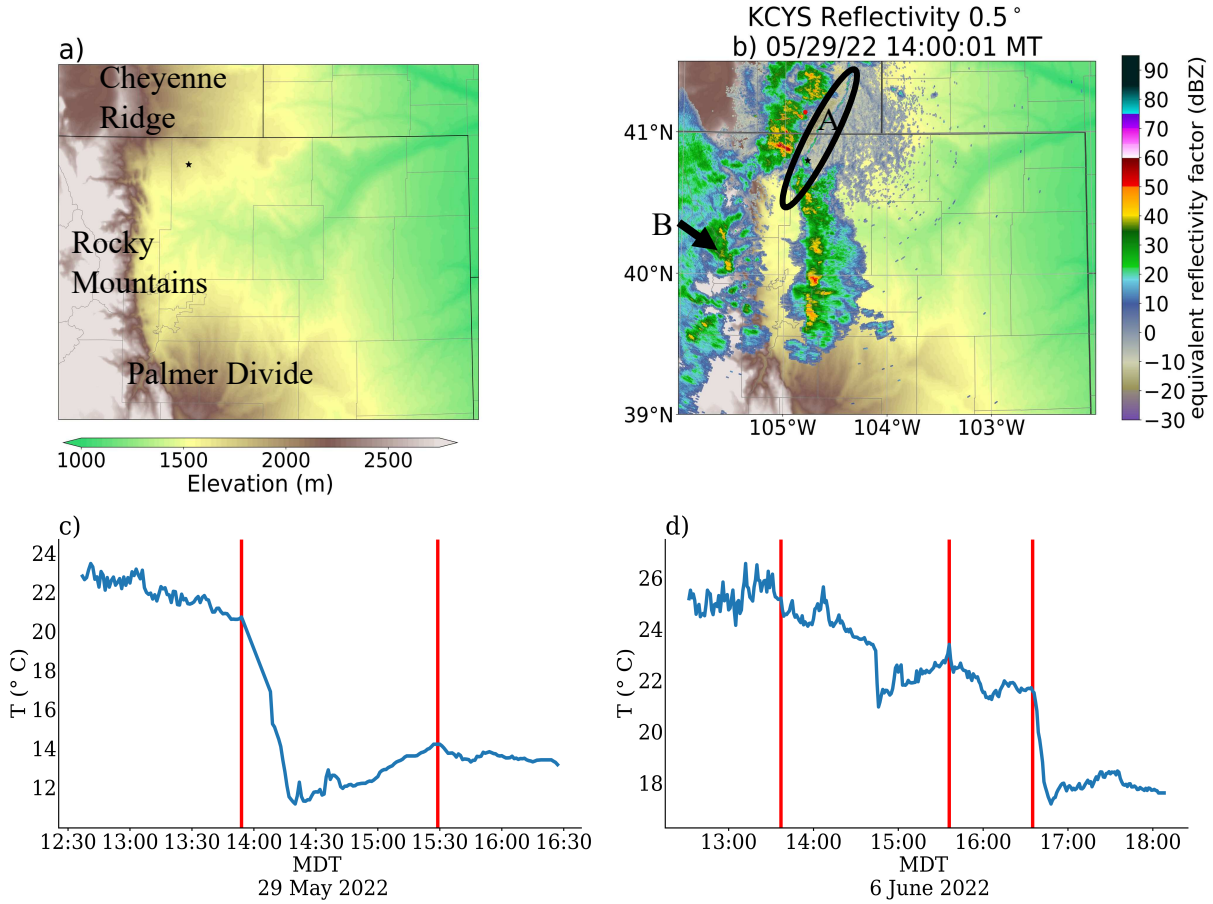

Figure 2.1: (a) A topographic map (m) of Northern Colorado and Southern Wyoming, with the location of CPER marked as the black star. (b) A radar image (dBZ) from the Cheyenne radar on 29 May 2022 at 1400 MT. The first squall line cold pool is labeled “A” and the squall line that produced the second cold pool is marked “B”. (c) Timeseries of temperature (°C) observed by the surface meteorological station on 29 May 2022 (blue line) with cold pool passages marked with red lines. (d) As in (c) but for 6 June 2022.

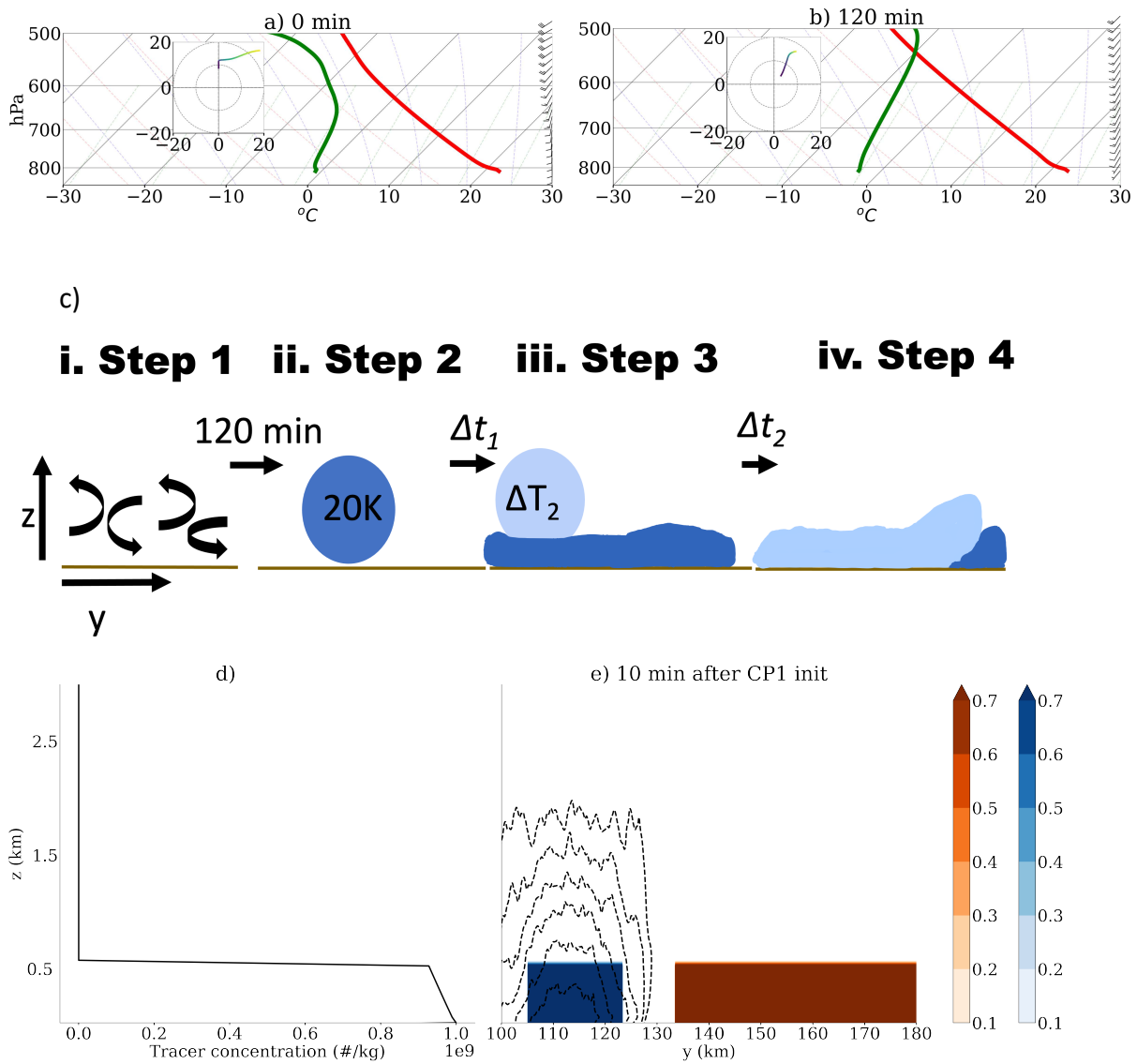

Figure 2.2: Visualizations of the modeling set up. (a) A sounding, hodograph from the surface to 3km AGL, and wind profile spatially-averaged over y=80 to y=120 km at the initialization time of the first cold pool (CP1). (b) As in (a), but at the initialization time of the second cold pool (CP2) in the CONTROL case. (c) A visualization of the steps in the two cold bubble experiments where (i) is the boundary layer development, (ii) is the release of the first bubble, (iii) is the release of the second bubble after the first has had time to spread out and evolve, and (iv) is the evolution of the first and second cold bubble. (d) A vertical profile of the initial tracer concentration (#/kg). (e) A y-z cross section of the initial tracer distribution for the environmental (orange shading) (unitless) and cold pool tracers (blue shading) that are normalized by the maximum initial tracer concentration, 1 x 10^9 kg^{-1}. Dashed contours are density potential temperature perturbation in intervals of -2 K, starting with -2K outwards then decreasing inwards, where the perturbation is defined as the perturbation from the environment far enough away to not be influenced by the cold pool (y=250-290 km).

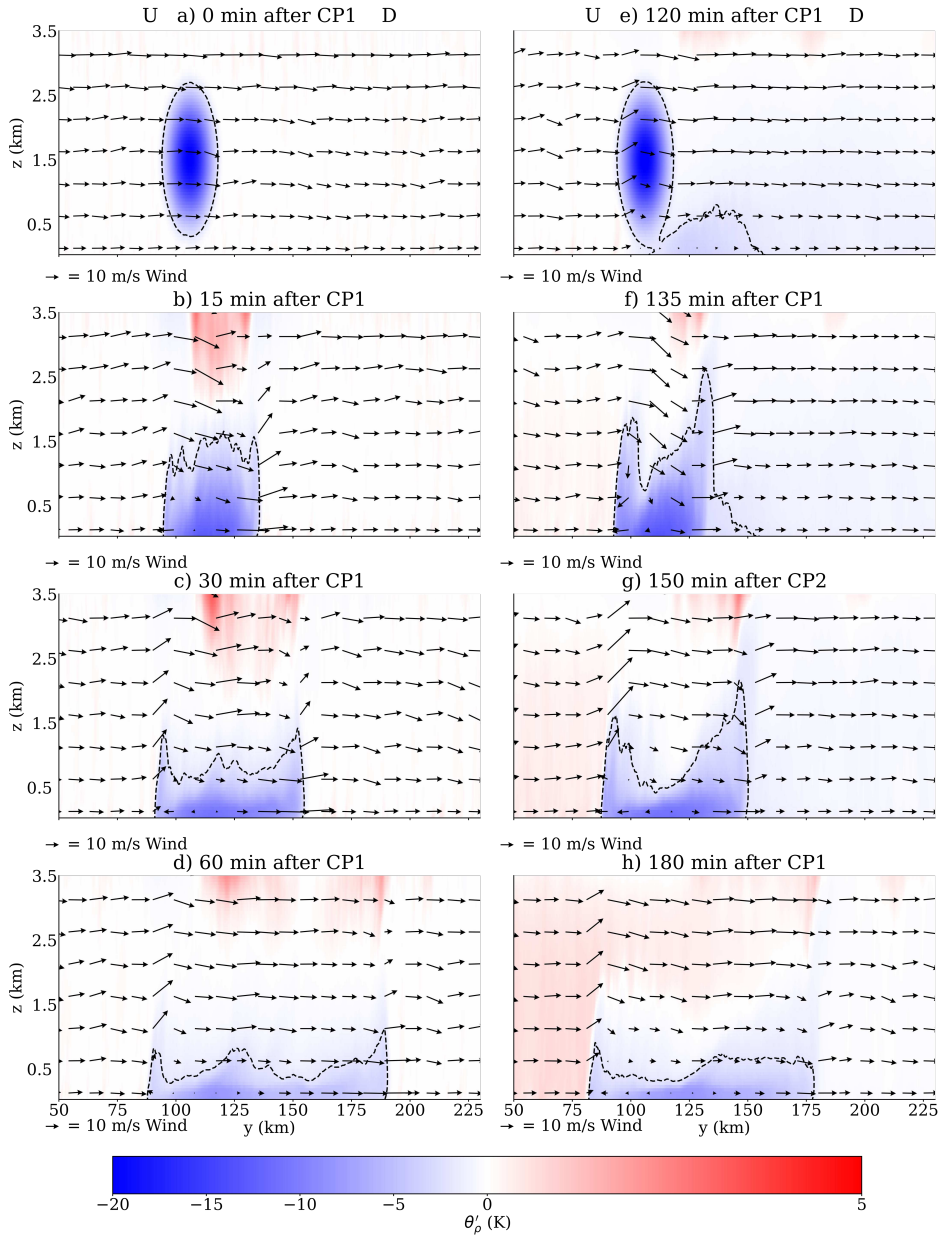

Figure 2.3: Y-z cross sections showing the temporal evolution of both cold pools in the CONTROL experiment. Density potential temperature perturbations (definition the same as in Figure 2.2e) (K) spatially averaged over x (shaded), <v,w> wind vectors (m/s), and the -2 K density potential temperature (dashed black contours) for (a) the initialization time of the first cold pool, (b) 15 minutes, (c) 30 minutes, (d) 60 minutes, (e) 120 minutes (0 minutes), (f) 135 minutes (15 minutes), (g) 150 minutes (30 minutes), and (h) 180 minutes (60 minutes) after the initialization of the first cold pool (time after the second cold pool). U denotes the upshear side of the cold pool while D denotes the downshear side of the cold pool.

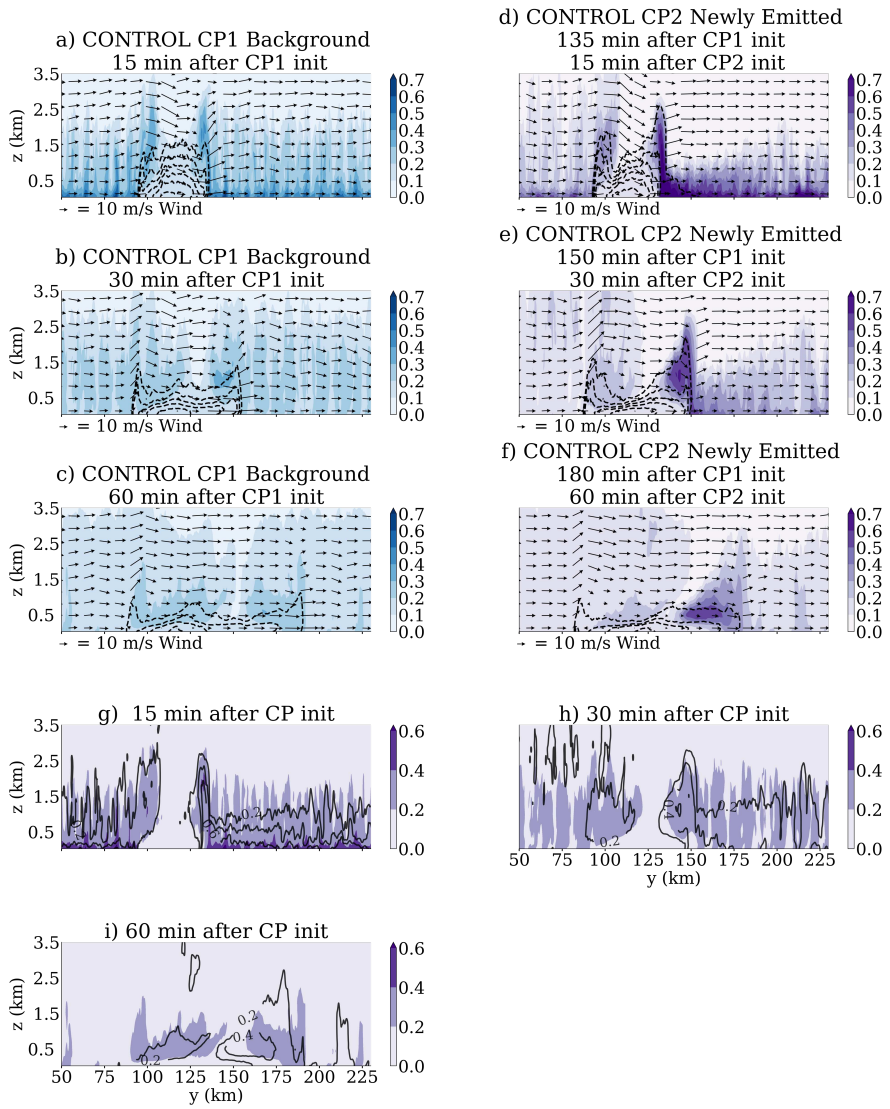

Figure 2.4: Y-z cross sections describing the temporal evolution of the background and newly emitted tracers in the two cold pools in the CONTROL experiment. The blue (purple) shading represents the background tracer (newly emitted tracer) (unitless) averaged in the x-direction and normalized by the maximum initial tracer concentration, the black dashed contours represent the x-averaged density potential temperature perturbations (K), and x-averaged <v,w> wind vectors (m/s) for (a) 15 minutes, (b) 30 minutes, (c) 60 minutes, (d) 135 minutes (15 minutes), (e) 150 minutes (30 minutes), and (f) 180 minutes (60 minutes) after the initialization of the first (second) cold pool. In (g)-(i) the purple shading is normalized tracer concentration of the newly emitted tracers (unitless) overlaid by the normalized background tracers (unitless) shown in black contours with intervals of 0.2 increasing inwards, for the time step relative to each cold pool's initialization: (g) 15 minutes, (h) 30 minutes, and (i) 60 minutes after initialization.

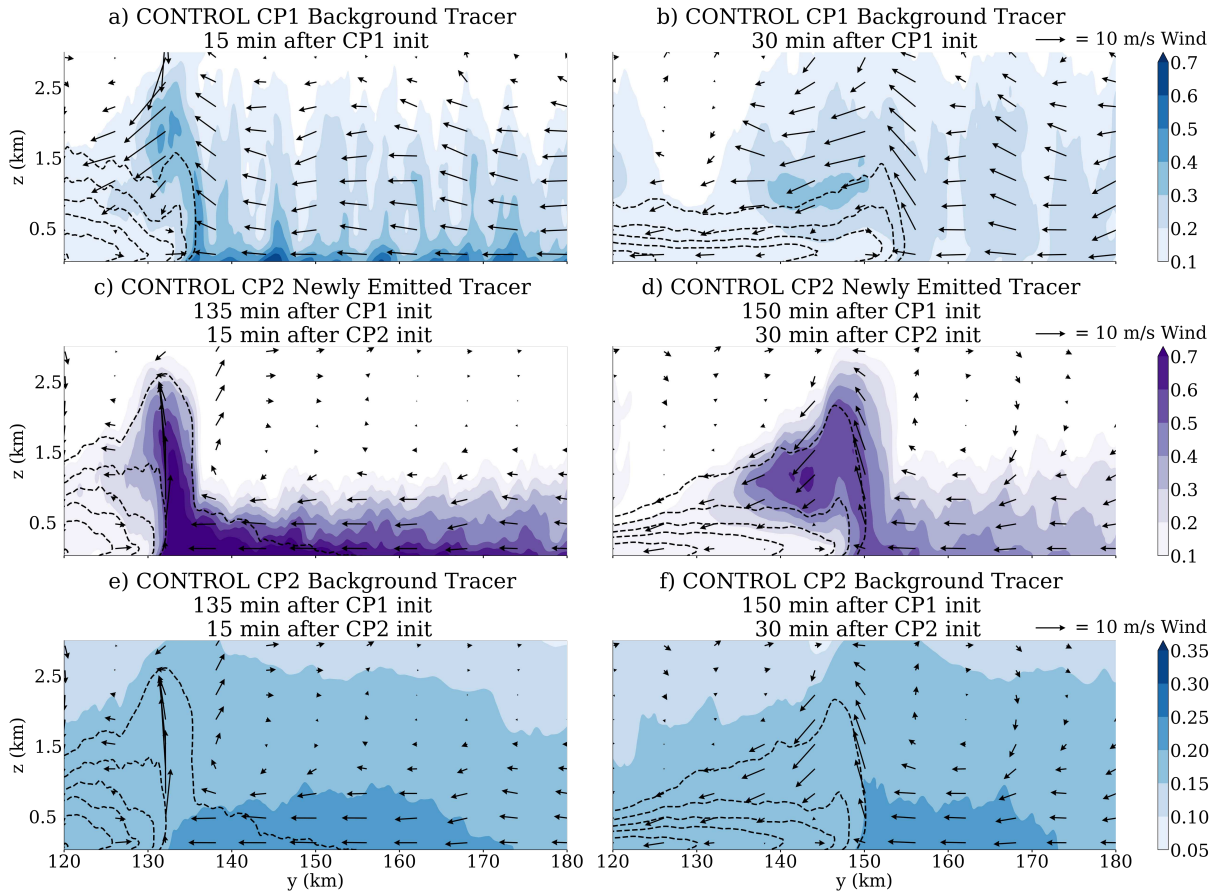

Figure 2.5: Y-z cross sections of the temporal evolution of the background and newly emitted tracers near the downshear leading edge of both cold pools in the CONTROL experiment. Similar to Figure 2.4a-f, but vectors are cold pool motion-relative winds (m/s), where the average cold pool propagation speed from 15-35 minutes was subtracted from the horizontal wind components. Panels (a) and (b) show normalized background tracer concentrations around the first cold pool in the train after (a) 15 minutes and (b) 30 minutes. Panels (c) and (d) show normalized newly emitted tracer concentrations in the second cold pool after (c) 15 minutes and (d) 30 minutes. Panels (e) and (f) are normalized background tracer concentrations associated with the second cold pool after (e) 15 minutes and (f) 30 minutes.

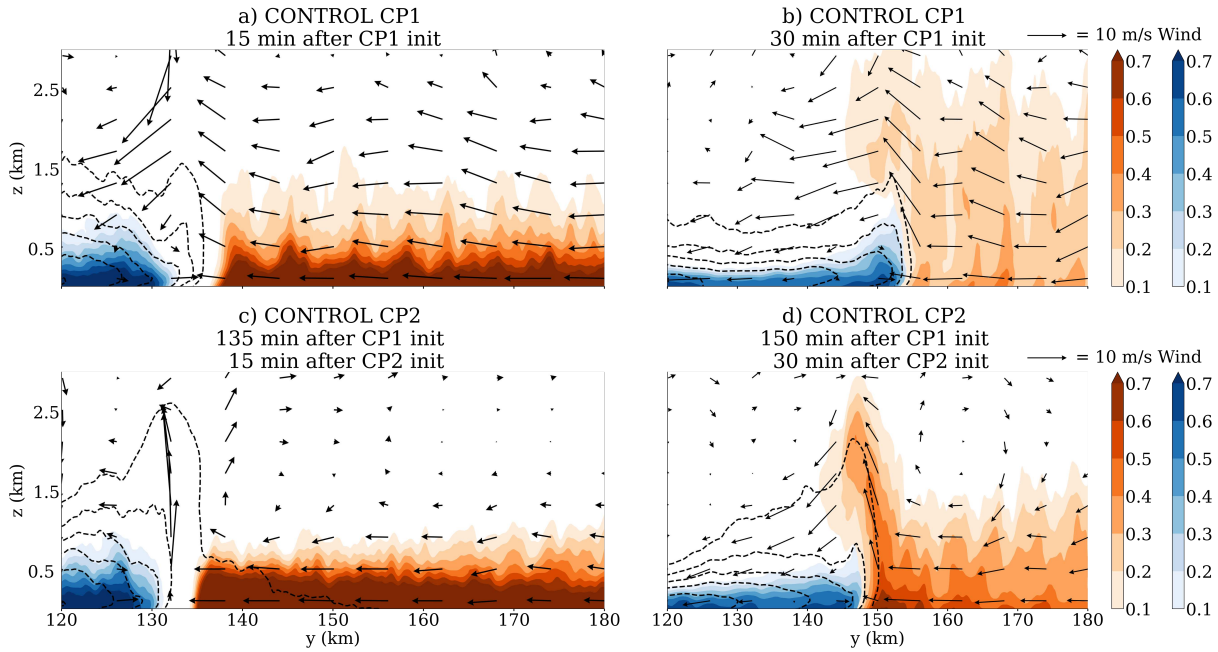

Figure 2.6: As in Figure 2.5(a-d), but for the normalized cold pool tracers (blue) and the normalized environmental tracers (orange).

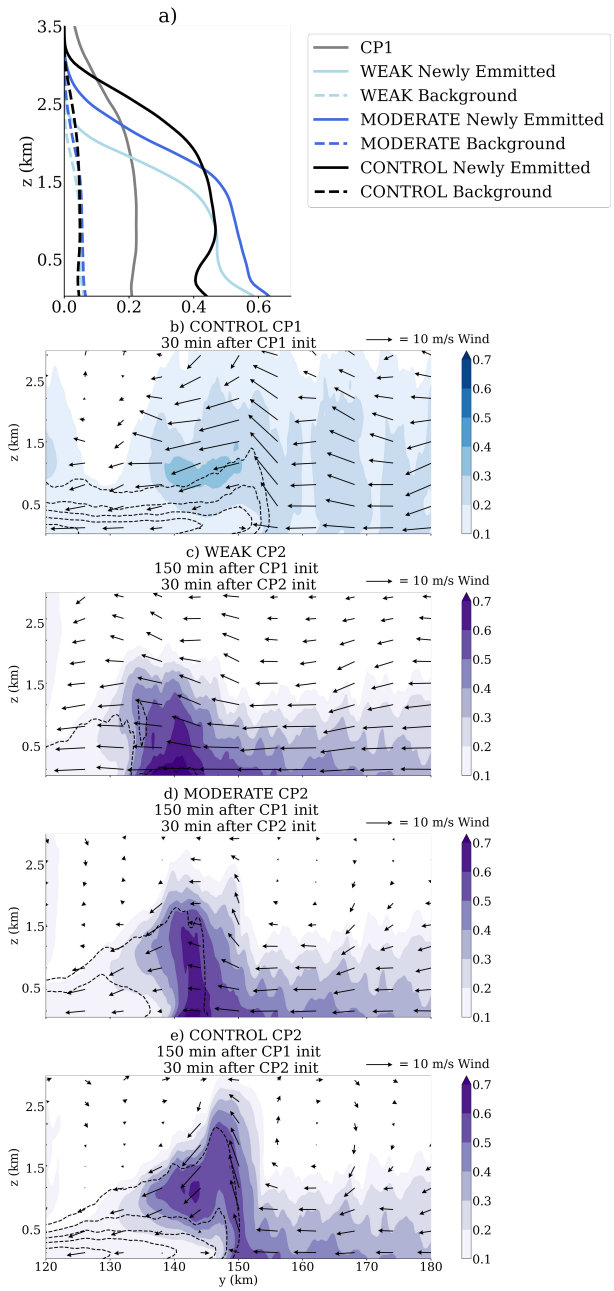

Figure 2.7: Results of the temperature deficit experiments for CP2. (a) Spatially averaged profiles of the normalized background tracer after 30 minutes of both CP1 and CP2 evolution. The averaging is performed across all of x and from 5 km ahead to 5 km behind the downshear cold pool's leading edge. Colors indicate different combinations of tracer and cold pools as indicated in the legend. The solid blue and black lines represent the newly emitted tracer lofted by each CP2 while the grey solid line represents the background tracer lofted by CP1. The dashed blue lines represent the background aerosols lofted by each CP2. Panels (b)-(e) are as in Figure 2.5b and 2.5d, but for (b) the normalized background tracer associated with CP 1, (c) the normalized newly emitted tracer associated with the WEAK CP2, (d) the normalized newly emitted tracer associated with the MODERATE CP2, and (e) the normalized newly emitted tracer associated with the CONTROL CP2.

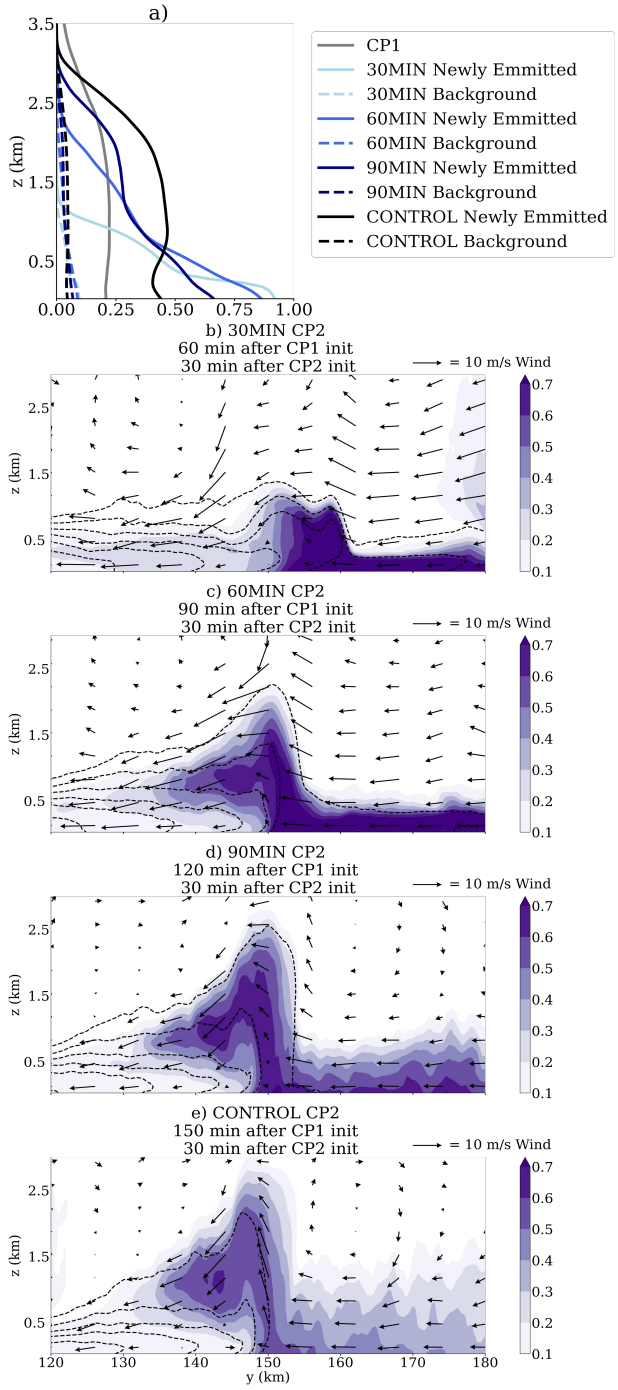

Figure 2.8: As in Figure 2.7, but for the timing sensitivity experiments for CP2. (a) As in Figure 2.7a, but for the timing sensitivity experiments. (b)-(e) as in Figure 2.7(b-e), but for (b) the normalized newly emitted tracer in the 30MIN CP2, (c) the normalized newly emitted tracer in the 60MIN CP2, (d) the normalized newly emitted tracer in the 90MIN CP2, and (e) the normalized newly emitted tracer in the CONTROL CP2.

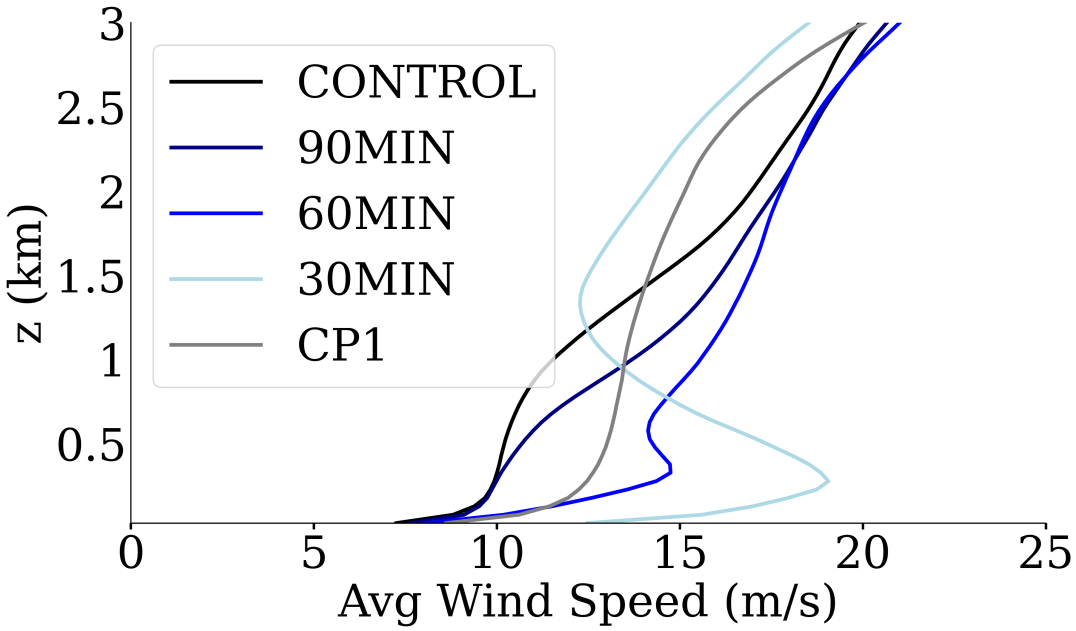

Figure 2.9: A vertical profile of the mean horizontal wind speed (m s^{-1}) ahead of the downshear side of CP1 (grey), the CP2s in experiments: 30MIN (light blue), 60MIN (blue), 90MIN (navy), and CONTROL. The profile is averaged from y=160 to y=180 km at t=30 minutes after each cold pool's initialization.

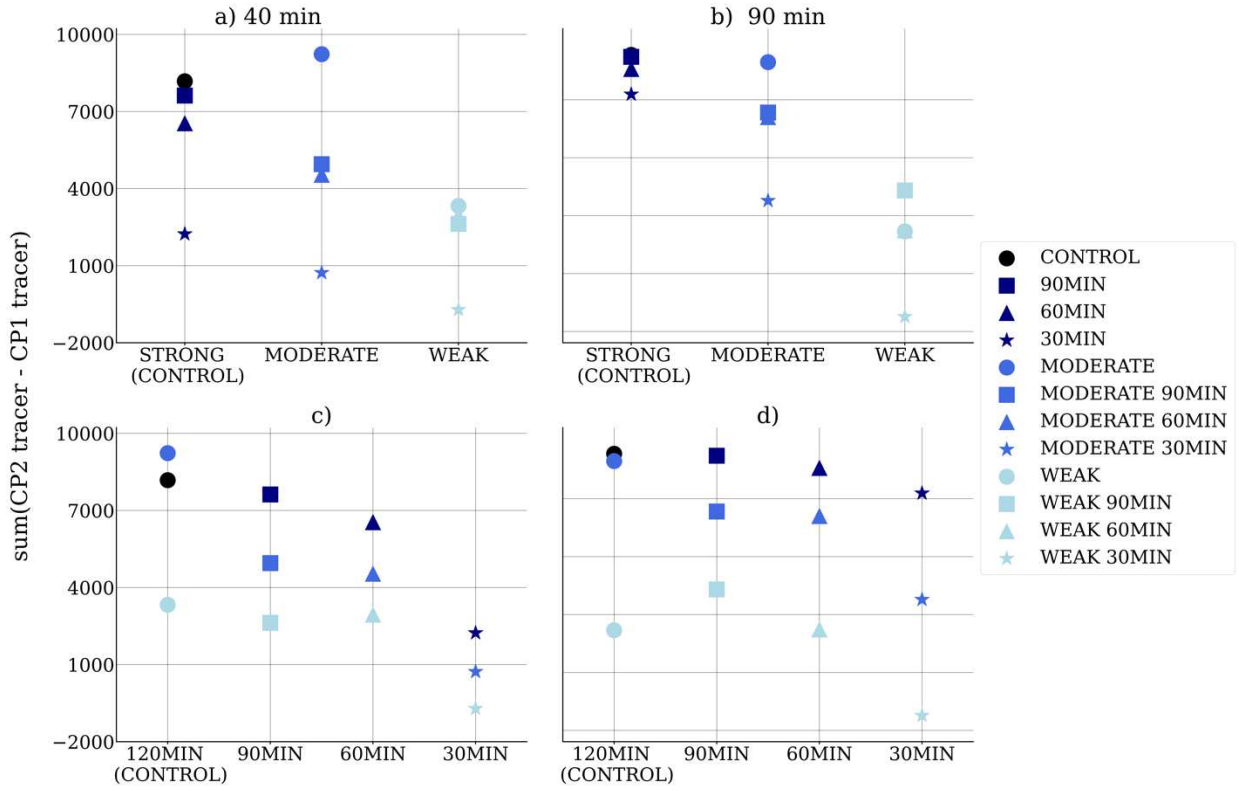

Figure 2.10: The sum of vertically integrated, spatially averaged, normalized newly emitted tracer concentration lofted by CP2 in all simulations, minus the vertically integrated, spatially averaged, normalized background tracer concentration lofted by CP1, after (a) and (c) 40 minutes of each cold pool's evolution, and (b) and (d) after 90 minutes of evolution. Tracer concentrations are integrated vertically from the surface to z=2.5 km and averaged spatially over 5 km ahead and 5 km behind the downshear leading edge of each cold pool. Each symbol corresponds to its shape in the legend. (a)-(b) categorizes by the initial temperature deficit in CP2, while (c)-(d) categorizes by time between cold pool initializations.

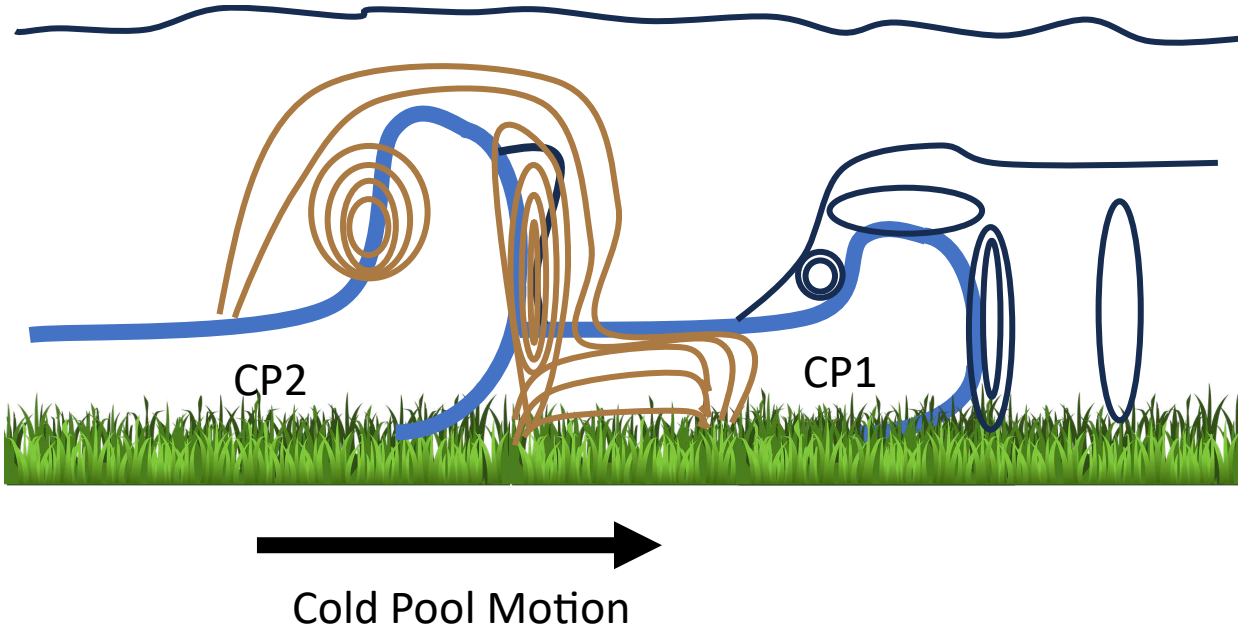

Figure 2.11: A schematic of the cold pool train lofting mechanisms and resultant tracer distributions identified in this study. The blue contours are the outlines of the cold pools, with the first cold pool labeled “CP1” and the second cold pool labeled “CP2”. The black contours represent the background tracer concentrations and the brown contours represent the newly emitted tracer concentrations, with the inner contours representing the greatest values.

Chapter 3: Conclusions

3.1 Summary of work

In this study, we investigate how the structure and dynamics differ among cold pools within cold pool trains – defined as cold pools passing through the same location on the same day without colliding – and how they alter the distribution of aerosols. During the BACS-I field campaign, we observed several cases where multiple cold pools passed over the field site on the same day during daylight hours, which motivated this study. In one of the BACS-I cases, two successive squall line cold pools were observed, which we use as a guide for the numerical model experiments presented in this study. We run a suite of Large Eddy Resolving simulations of two idealized, linearly-oriented cold pools. In the CONTROL simulation, the two cold pools, termed CP1 and CP2, have the same initialization properties – including a 20 K initial temperature deficit – and are initiated two hours apart. We conduct sensitivity tests with the strength of CP2, since we measured different relative cold pool strengths in the cold pool trains observed during BACS-I. Those sensitivity tests are named the MODERATE (10K) and WEAK (5K) cases. We also perform additional sensitivity tests to examine the impact of CP2's timing relative to CP1, in order to replicate the range of timings between two cold pools we observed during BACS-I. The timing experiments include 30 minutes ("30MIN"), 60 minutes ("60MIN"), and 90 minutes ("90MIN") between each cold pool, in addition to the CONTROL case (2 hours). To emulate the lofting of aerosols, we use passive tracers to represent different aerosol scenarios: background aerosols, aerosols emitted after the passage of CP1, within-cold pool aerosols, and environmental aerosols in the air ahead of the cold pool. This is the first study to numerically simulate cold pool trains and how they loft aerosols.

We find multiple physical processes that occur as a result of CP1's passage:

- CP1 stably stratifies the environment downshear of CP2, which, all else equal, would limit the depth of CP2's head and increase its propagation speed compared to CP1. The stabilization of the environment ahead of CP2 also increases the wind shear there by decreasing the near surface horizontal wind speeds. This increased wind shear deepens the head of CP2, and the weaker winds decrease its propagation speed. The stability and wind shear effects have opposite impacts on cold pool head depth and cold pool propagation speed (e.g. Liu and Moncrieff 1996; Rotunno et al. 1988; Xu 1992, Xu and Moncrieff 1994; Liu and Moncrieff 1996, 2000; Bryan and Rotunno 2014; Seigel and van den Heever 2012). However, in the simulations we conduct, the horizontal wind shear and mean wind speed have a stronger impact on CP2's downshear head depth and propagation speed than does stability, because the net effect is that CP2 propagates slower and has a deeper head on the downshear side as compared to CP1.
- The temperature deficit sensitivity tests show that the CONTROL CP2 has the deepest downshear head and greatest propagation speed, followed by the MODERATE then WEAK second cold pools, respectively. It has been shown previously that weaker cold pools propagate slower (Benjamin 1968), so this result is unsurprising. The timing sensitivity tests show the 90MIN CP2 has the deepest downshear head due to the greatest 0-3km vertical wind shear and lowest environmental stability compared to the CP2s in the 30MIN and 60MIN cases, while the CONTROL CP2 propagated the slowest. The CONTROL CP2 may

have propagated the slowest because it had the slowest mean advecting winds through its depth and had lower stability than the other CP2s in the timing sensitivity experiments.

In examining the impacts of the CP1 and CP2 properties on aerosol lofting, which is represented by passive tracers, we find that:

- CP1 lofts the most *background* tracer at its leading *downshear* edge. The CONTROL CP2 case lofts less than half of the background tracer compared to CP1, a result that is similar across all of the sensitivity tests. The tracer lofted by the cold pools' leading edges originate in the environment ahead of the cold pool, while the tracer originating in the cold pool remains trapped inside the cold pool. However, CP2 can loft a substantially greater concentration of tracer *newly emitted* after the CP1 passage, compared to CP1's lofting of the background tracer. These changes in lofting are driven by the stable stratification of the environment ahead of CP2 induced by CP1, which traps the newly emitted tracer near the surface as opposed to being vertically mixed within the boundary layer, thereby allowing for a greater concentration of tracer to be lofted along CP2's downshear leading edge. At the *upshear* edge of the cold pools, CP2 lofts a similar amount of newly emitted tracer as CP1 lofts of the background tracer because the tracers are similarly vertically mixed within the upshear environment. CP1 does not propagate far in the upshear direction due to the strong wind speeds opposing it, and this causes the upshear environment ahead of both CP1 and CP2 to remain similarly unstable.

- The cold pool strength sensitivity tests show that the CONTROL CP2 transports the most newly emitted tracer aloft, followed by the MODERATE, and lastly the WEAK CP2. There is a linear trend in tracer lofting as CP2's initial temperature deficit decreases because the strength of the cold pool is related to the updraft intensity at the cold pool's edges.
- The timing sensitivity tests show that the CONTROL CP2 lofts the most newly emitted tracer, followed by the 90MIN, 60MIN, and 30MIN cases. The CONTROL CP2 lofts the most newly emitted tracer because its environment is the most destabilized of the CP2 timing sensitivity experiments. Overall, the temperature deficit of CP2 plays a more important role in tracer lofting than the timing between CP1 and CP2 for the lifetime of the cold pools. The temperature deficit becomes more important for CP2 as timing between cold pools increases.

However, while the stabilization effect of CP1 is more important for tracer lofting by CP2, the changes in the wind profile caused by the stabilization is more important for the dynamics of CP2.

These results have implications for potential transport and ingestion of aerosol into convective storms, where aerosols such as dust and biological particulates may serve as INP and CCN, subsequently affecting storm microphysics and dynamics. These results also highlight the need to include interactive aerosols, as well as the interactions and feedbacks between such aerosols and cold pool dynamics in forecast models, if aerosol distributions and their subsequent impacts on air quality and convective processes are to be accurately forecasted.

3.2 Future work

Our results show that there are substantive differences between how cold pools in a cold pool train loft aerosol. In this study, we initialize cold pools in a high wind shear environment. The differences in aerosol lofting and dynamics may not be as large if the initial environment has low wind shear. Additionally, the effects of the first cold pool on the environment ahead of the second cold pool may not be as large if the first cold pool is weaker. These would be worthwhile avenues of future research pursuits. Additionally, different storm types and their associated cold pools may impact the aerosol lofting by the cold pools comprising cold pool trains, and to what extent the aerosols lofted by different cold pools in the train may be ingested into the parent or subsequent convective storms. In future modeling studies, aerosols and their associated processes should be included, since aerosols may settle out or undergo wet deposition from precipitation from storms and therefore the amount available to a secondary storm may be reduced. Furthermore, as cold pool impacts on convection are variable under different environments (Rotunno et al. 1988; Falk and van den Heever 2023; Grant et al. 2018; Weisman and Rotunno 2004), it would be beneficial to conduct modeling studies of cold pool trains in moist tropical regimes, since here we only simulate cold pool trains in a dry midlatitude environment.

Recent advances in observing platforms may further our understanding of cold pool trains and their impact on aerosol lofting. For instance, there have been recent studies that have used meteorological towers to study cold pools (e.g., Kirsch et al. 2021; Kruse et al. 2022; Mai et al. 2023) and aerosols (e.g., Sun et al. 2020). These towers may be able to observe the vertical structure of cold pools in cold pool trains in different environments and the aerosols within them. Such observations would enhance our knowledge of the variability of cold pool properties in cold pool trains and would be useful in verifying the results of this modeling study.

Furthermore, ongoing analysis of BACS-I and BACS-II data will provide insight into the properties of cold pools in cold pool trains and their impacts on aerosol concentrations, both at the surface and aloft. During BACS-I and BACS-II, observations of cold pools and cold pool trains were gathered from radiosondes, small uncrewed arial vehicles (drones), and a surface meteorological station. Future research will focus on using temperature, humidity, pressure, and wind data collected to examine the spatial and temporal variability of cold pools in cold pool trains. Vertically resolved aerosol size distribution data were also collected by the drones during BACS-I and BACS-II. Analysis of these observations from BACS-I and BACS-II will provide fascinating insights into the observed variability of properties in cold pool trains and their impacts on aerosol lofting.

References

Baddock, M. C., C. L. Strong, P. S. Murray, and G. H. McTainsh, 2013: Aeolian dust as a transport hazard. *Atmospheric Environment*, **71**, 7–14, https://doi.org/10.1016/j.atmosenv.2013.01.042.

Bannister, T., and Coauthors, 2020: Are convergence lines associated with high asthma presentation days? A case-control study in Melbourne, Australia. *Science of The Total Environment*, **737**, 140263, https://doi.org/10.1016/j.scitotenv.2020.140263.

Beggs, P. J., 2017: Allergen aerosol from pollen-nucleated precipitation: A novel thunderstorm asthma trigger. *Atmospheric Environment*, **152**, 455–457, https://doi.org/10.1016/j.atmosenv.2016.12.045.

Benjamin, T. B., 1968: Gravity currents and related phenomena. *Journal of Fluid Mechanics*, **31**, 209–248, https://doi.org/10.1017/S0022112068000133.

Böing, S. J., H. J. J. Jonker, A. P. Siebesma, and W. W. Grabowski, 2012: Influence of the Subcloud Layer on the Development of a Deep Convective Ensemble. *Journal of the Atmospheric Sciences*, **69**, 2682–2698, https://doi.org/10.1175/JAS-D-11-0317.1.

Bou Karam, D., C. Flamant, P. Tulet, J.-P. Chaboureau, A. Dabas, and M. C. Todd, 2009: Estimate of Sahelian dust emissions in the intertropical discontinuity region of the West African Monsoon. *Journal of Geophysical Research: Atmospheres*, **114**, https://doi.org/10.1029/2008JD011444.

Bryan, G. H., and R. Rotunno, 2014: The Optimal State for Gravity Currents in Shear. *Journal of the Atmospheric Sciences*, **71**, 448–468, https://doi.org/10.1175/JAS-D-13-0156.1.

——, J. C. Wyngaard, and J. M. Fritsch, 2003: Resolution Requirements for the Simulation of Deep Moist Convection. *Monthly Weather Review*, **131**, 2394–2416, https://doi.org/10.1175/1520-0493(2003)131<2394:RRFTSO>2.0.CO;2.

——, D. A. Ahijevych, C. A. Davis, M. L. Weisman, and R. Przybylinski, 2004: An assessment of convective system structure, cold pool properties, and environmental shear using observations from BAMEX. 22nd Conference on Severe Local Storms.

——, J. C. Knievel, and M. D. Parker, 2006: A Multimodel Assessment of RKW Theory's Relevance to Squall-Line Characteristics. *Monthly Weather Review*, **134**, 2772–2792, https://doi.org/10.1175/MWR3226.1.

Bukowski, J., and S. C. van den Heever, 2021: Direct Radiative Effects in Haboobs. *Journal of Geophysical Research: Atmospheres*, **126**, e2021JD034814, https://doi.org/10.1029/2021JD034814.

Bukowski, J., and S. C. van den Heever, 2022: The Impact of Land Surface Properties on Haboobs and Dust Lofting. *Journal of the Atmospheric Sciences*, **79**, 3195–3218, https://doi.org/10.1175/JAS-D-22-0001.1.

Burkart, J., J. Gratzl, T. M. Seifried, P. Bieber, and H. Grothe, 2021: *Subpollen particles (SPP) of birch as carriers of ice nucleating macromolecules*. Biogeochemistry: Air - Land Exchange,.

Byers, H. R., and R. R. Braham, 1949: The Thunderstorm: Report of the Thunderstorm Project. *U.S. Government Printing Office*, 287.

Cotton, W. R., and Coauthors, 2003: RAMS 2001: Current status and future directions. *Meteorol Atmos Phys*, **82**, 5–29, https://doi.org/10.1007/s00703-001-0584-9.

D'Amato, G., I. Annesi-Maesano, L. Cecchi, and M. D'Amato, 2019: Latest news on relationship between thunderstorms and respiratory allergy, severe asthma, and deaths for asthma. *Allergy*, **74**, 9–11, https://doi.org/10.1111/all.13616.

DeMott, P. J., K. Sassen, M. R. Poellot, D. Baumgardner, D. C. Rogers, S. D. Brooks, A. J. Prenni, and S. M. Kreidenweis, 2003: African dust aerosols as atmospheric ice nuclei. *Geophysical Research Letters*, **30**, https://doi.org/10.1029/2003GL017410.

Diehl, K., C. Quick, S. Matthias-Maser, S. K. Mitra, and R. Jaenicke, 2001: The ice nucleating ability of pollen: Part I: Laboratory studies in deposition and condensation freezing modes. *Atmospheric Research*, **58**, 75–87, https://doi.org/10.1016/S0169-8095(01)00091-6.

Dreischmeier, K., C. Budke, L. Wiehemeier, T. Kottke, and T. Koop, 2017: Boreal pollen contain ice-nucleating as well as ice-binding 'antifreeze' polysaccharides. *Sci Rep*, **7**, 41890, https://doi.org/10.1038/srep41890.

Droegemeier, K. K., and R. B. Wilhelmson, 1985a: Three-Dimensional Numerical Modeling of Convection Produced by Interacting Thunderstorm Outflows. Part I: Control Simulation and Low-Level Moisture Variations. *Journal of the Atmospheric Sciences*, **42**, 2381–2403, https://doi.org/10.1175/1520-0469(1985)042<2381:TDNMOC>2.0.CO;2.

——, and ——, 1985b: Three-Dimensional Numerical Modeling of Convection Produced by Interacting Thunderstorm Outflows. Part II: Variations in Vertical Wind Shear. *Journal of the Atmospheric Sciences*, **42**, 2404–2414, https://doi.org/10.1175/1520-0469(1985)042<2404:TDNMOC>2.0.CO;2.

Emmanuel, K. A., 1994: *Atmospheric Convection*. 1st ed. University of Oxford Press, 592 pp.

Emmerson, K. M., and Coauthors, 2021: Atmospheric modelling of grass pollen rupturing mechanisms for thunderstorm asthma prediction. *PLOS ONE*, **16**, e0249488, https://doi.org/10.1371/journal.pone.0249488.

Falk, N. M., and S. C. van den Heever, 2023: Environmental Modulation of Mechanical and Thermodynamic Forcing from Cold Pool Collisions. *Journal of the Atmospheric Sciences*, **80**, 375–395, https://doi.org/10.1175/JAS-D-22-0020.1.

Feng, Z., S. Hagos, A. K. Rowe, C. D. Burleyson, M. N. Martini, and S. P. de Szoeke, 2015: Mechanisms of convective cloud organization by cold pools over tropical warm ocean during the AMIE/DYNAMO field campaign. *Journal of Advances in Modeling Earth Systems*, **7**, 357–381, https://doi.org/10.1002/2014MS000384.

Field, P. R., O. Möhler, P. Connolly, M. Krämer, R. Cotton, A. J. Heymsfield, H. Saathoff, and M. Schnaiter, 2006: Some ice nucleation characteristics of Asian and Saharan desert dust. *Atmospheric Chemistry and Physics*, **6**, 2991–3006, https://doi.org/10.5194/acp-6-2991-2006.

Flamant, C., J.-P. Chaboureau, D. J. Parker, C. M. Taylor, J.-P. Cammas, O. Bock, F. Timouk, and J. Pelon, 2007: Airborne observations of the impact of a convective system on the planetary boundary layer thermodynamics and aerosol distribution in the inter-tropical discontinuity region of the West African Monsoon. *Quarterly Journal of the Royal Meteorological Society*, **133**, 1175–1189, https://doi.org/10.1002/qj.97.

Fujita, T.T., 1978: *Manual of downburst identification for project NIMROD.* University of Chicago, 104 pp.

Garcia-Carreras, L., and Coauthors, 2013: The impact of convective cold pool outflows on model biases in the Sahara. *Geophysical Research Letters*, **40**, 1647–1652, https://doi.org/10.1002/grl.50239.

Gentine, P., A. Garelli, S.-B. Park, J. Nie, G. Torri, and Z. Kuang, 2016: Role of surface heat fluxes underneath cold pools. *Geophysical Research Letters*, **43**, 874–883, https://doi.org/10.1002/2015GL067262.

Goudie, A. S., 2014: Desert dust and human health disorders. *Environment International*, **63**, 101–113, https://doi.org/10.1016/j.envint.2013.10.011.

Grant, L. D., and S. C. van den Heever, 2016: Cold pool dissipation. *Journal of Geophysical Research: Atmospheres*, **121**, 1138–1155, https://doi.org/10.1002/2015JD023813.

——, and ——, 2018: Cold Pool-Land Surface Interactions in a Dry Continental Environment. *Journal of Advances in Modeling Earth Systems*, **10**, 1513–1526, https://doi.org/10.1029/2018MS001323.

——, T. P. Lane, and S. C. van den Heever, 2018: The Role of Cold Pools in Tropical Oceanic Convective Systems. *Journal of the Atmospheric Sciences*, **75**, 2615–2634, https://doi.org/10.1175/JAS-D-17-0352.1.

Grote, M., S. Vrtala, V. Niederberger, R. Wiermann, R. Valenta, and R. Reichelt, 2001: Release of allergen-bearing cytoplasm from hydrated pollen: A mechanism common to a variety

of grass (Poaceae) species revealed by electron microscopy. *Journal of Allergy and Clinical Immunology*, **108**, 109–115, https://doi.org/10.1067/mai.2001.116431.

——, R. Valenta, and R. Reichelt, 2003: Abortive pollen germination: A mechanism of allergen release in birch, alder, and hazel revealed by immunogold electron microscopy. *Journal of Allergy and Clinical Immunology*, **111**, 1017–1023, https://doi.org/10.1067/mai.2003.1452.

Gute, E., and J. P. D. Abbatt, 2018: Oxidative Processing Lowers the Ice Nucleation Activity of Birch and Alder Pollen. *Geophysical Research Letters*, **45**, 1647–1653, https://doi.org/10.1002/2017GL076357.

Hirt, M., G. C. Craig, S. A. K. Schäfer, J. Savre, and R. Heinze, 2020: Cold-pool-driven convective initiation: using causal graph analysis to determine what convection-permitting models are missing. *Quarterly Journal of the Royal Meteorological Society*, **146**, 2205–2227, https://doi.org/10.1002/qj.3788.

Hughes, D. D., C. B. A. Mampage, L. M. Jones, Z. Liu, and E. A. Stone, 2020: Characterization of Atmospheric Pollen Fragments during Springtime Thunderstorms. *Environ. Sci. Technol. Lett.*, **7**, 409–414, https://doi.org/10.1021/acs.estlett.0c00213.

Intrieri, J. M., A. J. Bedard, and R. M. Hardesty, 1990: Details of Colliding Thunderstorm Outflows as Observed by Doppler Lidar. *Journal of the Atmospheric Sciences*, **47**, 1081–1099, https://doi.org/10.1175/1520-0469(1990)047<1081:DOCTOA>2.0.CO;2.

Keulegan, G. H., 1958: *Twelfth Progress Report on Model Laws for Density Currents: The Motion of Saline Fronts in Still Water*. U.S. Department of Commerce, National Bureau of Standards, 108 pp.

Khairoutdinov, M., and D. Randall, 2006: High-Resolution Simulation of Shallow-to-Deep Convection Transition over Land. *Journal of the Atmospheric Sciences*, **63**, 3421–3436, https://doi.org/10.1175/JAS3810.1.

Kirsch, B., F. Ament, and C. Hohenegger, 2021: Convective Cold Pools in Long-Term Boundary Layer Mast Observations. *Monthly Weather Review*, **149**, 811–820, https://doi.org/10.1175/MWR-D-20-0197.1.

Knippertz, P., J. Trentmann, and A. Seifert, 2009a: High-resolution simulations of convective cold pools over the northwestern Sahara. *Journal of Geophysical Research: Atmospheres*, **114**, https://doi.org/10.1029/2008JD011271.

——, ——, and ——, 2009b: High-resolution simulations of convective cold pools over the northwestern Sahara. *Journal of Geophysical Research: Atmospheres*, **114**, https://doi.org/10.1029/2008JD011271.

Kruse, I. L., J. O. Haerter, and B. Meyer, 2022: Cold pools over the Netherlands: A statistical study from tower and radar observations. *Quarterly Journal of the Royal Meteorological Society*, **148**, 711–726, https://doi.org/10.1002/qj.4223.

Kurowski, M. J., K. Suselj, W. W. Grabowski, and J. Teixeira, 2018: Shallow-to-Deep Transition of Continental Moist Convection: Cold Pools, Surface Fluxes, and Mesoscale Organization. *Journal of the Atmospheric Sciences*, **75**, 4071–4090, https://doi.org/10.1175/JAS-D-18-0031.1.

Langhans, W., and D. M. Romps, 2015: The origin of water vapor rings in tropical oceanic cold pools. *Geophysical Research Letters*, **42**, 7825–7834, https://doi.org/10.1002/2015GL065623.

Lima, M. A., and J. W. Wilson, 2008: Convective Storm Initiation in a Moist Tropical Environment. *Monthly Weather Review*, **136**, 1847–1864, https://doi.org/10.1175/2007MWR2279.1.

Linden, P. F., and J. E. Simpson, 1986: Gravity-driven flows in a turbulent fluid. *Journal of Fluid Mechanics*, **172**, 481–497, https://doi.org/10.1017/S0022112086001829.

Liu, C., and M. W. Moncrieff, 1996: A Numerical Study of the Effects of Ambient Flow and Shear On Density Currents. *Monthly Weather Review*, **124**, 2282–2303, https://doi.org/10.1175/1520-0493(1996)124<2282:ANSOTE>2.0.CO;2.

——, and ——, 2000: Simulated Density Currents in Idealized Stratified Environments. *Monthly Weather Review*, **128**, 1420–1437, https://doi.org/10.1175/1520-0493(2000)128<1420:SDCIIS>2.0.CO;2.

Mai, C., Y. Du, and M. Li, 2023: Processes of Colliding Cold Pools Derived from a 356-m High Shenzhen Met-Tower during an Extremely Heavy Rainfall Event. *Monthly Weather Review*, **1**, https://doi.org/10.1175/MWR-D-22-0214.1.

Marks, G. B., J. R. Colquhoun, S. T. Girgis, M. H. Koski, A. B. A. Treloar, P. Hansen, S. H. Downs, and N. G. Car, 2001: Thunderstorm outflows preceding epidemics of asthma during spring and summer. *Thorax*, **56**, 468–471, https://doi.org/10.1136/thx.56.6.468.

Meyer, B., and J. O. Haerter, 2020: Mechanical Forcing of Convection by Cold Pools: Collisions and Energy Scaling. *Journal of Advances in Modeling Earth Systems*, **12**, e2020MS002281, https://doi.org/10.1029/2020MS002281.

Middleton, G. V., 1966: Experiments on density and turbidity currents: ii. uniform flow of density currents. *Can. J. Earth Sci.*, **3**, 627–637, https://doi.org/10.1139/e66-044.

Middleton, N. J., 2017: Desert dust hazards: A global review. *Aeolian Research*, **24**, 53–63, https://doi.org/10.1016/j.aeolia.2016.12.001.

Miguel, A. G., P. E. Taylor, J. House, M. M. Glovsky, and R. C. Flagan, 2006: Meteorological Influences on Respirable Fragment Release from Chinese Elm Pollen. *Aerosol Science and Technology*, **40**, 690–696, https://doi.org/10.1080/02786820600798869.

Miller, S. D., A. P. Kuciauskas, M. Liu, Q. Ji, J. S. Reid, D. W. Breed, A. L. Walker, and A. A. Mandoos, 2008: Haboob dust storms of the southern Arabian Peninsula. *Journal of Geophysical Research: Atmospheres*, **113**, https://doi.org/10.1029/2007JD008550.

——, and Coauthors, 2019: A Tale of Two Dust Storms: analysis of a complex dust event in the Middle East. *Atmospheric Measurement Techniques*, **12**, 5101–5118, https://doi.org/10.5194/amt-12-5101-2019.

Moncrieff, M. W., and C. Liu, 1999: Convection Initiation by Density Currents: Role of Convergence, Shear, and Dynamical Organization. *Monthly Weather Review*, **127**, 2455–2464, https://doi.org/10.1175/1520-0493(1999)127<2455:CIBDCR>2.0.CO;2.

Murray, B. J., D. O'Sullivan, J. D. Atkinson, and M. E. Webb, 2012: Ice nucleation by particles immersed in supercooled cloud droplets. *Chem. Soc. Rev.*, **41**, 6519–6554, https://doi.org/10.1039/C2CS35200A.

Neumaier, C.A., L.D. Grant, S.C. van den Heever, B.D. Ascher, J. Escobedo, N.M. Falk, S.W. Freeman, G.R. Leung, A.C. Mazurek, D.S. Veloso-Aguila, P.J. DeMott, S.M. Kreidenweis, R.J. Perkins, and E.A. Stone, 2023: Cold Pool Train Dynamics and Transport. *Journal of the Atmospheric Sciences*. In prep.

Newson, R., D. Strachan, E. Archibald, J. Emberlin, P. Hardaker, and C. Collier, 1997: Effect of thunderstorms and airborne grass pollen on the incidence of acute asthma in England, 1990-94. *Thorax*, **52**, 680–685, https://doi.org/10.1136/thx.52.8.680.

Prenni, A. J., and Coauthors, 2007: Examinations of ice formation processes in Florida cumuli using ice nuclei measurements of anvil ice crystal particle residues. *Journal of Geophysical Research: Atmospheres*, **112**, https://doi.org/10.1029/2006JD007549.

Pummer, B. G., H. Bauer, J. Bernardi, S. Bleicher, and H. Grothe, 2012: Suspendable macromolecules are responsible for ice nucleation activity of birch and conifer pollen. *Atmospheric Chemistry and Physics*, **12**, 2541–2550, https://doi.org/10.5194/acp-12-2541-2012.

Purdom, J. F. W., 1976: Some Uses of High-Resolution GOES Imagery in the Mesoscale Forecasting of Convection and Its Behavior. *Monthly Weather Review*, **104**, 1474–1483, https://doi.org/10.1175/1520-0493(1976)104<1474:SUOHRG>2.0.CO;2.

——, 1982: Subjective interpretation of geostationary satellite data for nowcasting. *Nowcasting*, 149–166.

Roberts, A. J., and P. Knippertz, 2014: The formation of a large summertime Saharan dust plume: Convective and synoptic-scale analysis. *Journal of Geophysical Research: Atmospheres*, **119**, 1766–1785, https://doi.org/10.1002/2013JD020667.

Rotunno, R., J. B. Klemp, and M. L. Weisman, 1988: A Theory for Strong, Long-Lived Squall Lines. *Journal of the Atmospheric Sciences*, **45**, 463–485, https://doi.org/10.1175/1520-0469(1988)045<0463:ATFSLL>2.0.CO;2.

Saleeby, S. M., and S. C. van den Heever, 2013: Developments in the CSU-RAMS Aerosol Model: Emissions, Nucleation, Regeneration, Deposition, and Radiation. *Journal of Applied Meteorology and Climatology*, **52**, 2601–2622, https://doi.org/10.1175/JAMC-D-12-0312.1.

Schlemmer, L., and C. Hohenegger, 2016: Modifications of the atmospheric moisture field as a result of cold-pool dynamics. *Quarterly Journal of the Royal Meteorological Society*, **142**, 30–42, https://doi.org/10.1002/qj.2625.

Seigel, R. B., and S. C. van den Heever, 2012a: Dust Lofting and Ingestion by Supercell Storms. *Journal of the Atmospheric Sciences*, **69**, 1453–1473, https://doi.org/10.1175/JAS-D-11-0222.1.

——, and ——, 2012b: Simulated Density Currents beneath Embedded Stratified Layers. *Journal of the Atmospheric Sciences*, **69**, 2192–2200, https://doi.org/10.1175/JAS-D-11-0255.1.

Simpson, J. E., 1969: A comparison between laboratory and atmospheric density currents. *Quarterly Journal of the Royal Meteorological Society*, **95**, 758–765, https://doi.org/10.1002/qj.49709540609.

——, Gravity Currents in the Environment and the Laboratory. **2nd Edition Cambridge University Press**, 244.

Slingo, A., and Coauthors, 2006: Observations of the impact of a major Saharan dust storm on the atmospheric radiation balance. *Geophysical Research Letters*, **33**, https://doi.org/10.1029/2006GL027869.

Sokolik, I. N., and O. B. Toon, 1996: Direct radiative forcing by anthropogenic airborne mineral aerosols. *Nature*, **381**, 681–683, https://doi.org/10.1038/381681a0.

Steiner, A. L., S. D. Brooks, C. Deng, D. C. O. Thornton, M. W. Pendleton, and V. Bryant, 2015: Pollen as atmospheric cloud condensation nuclei. *Geophysical Research Letters*, **42**, 3596–3602, https://doi.org/10.1002/2015GL064060.

Stone, E. A., C. B. A. Mampage, D. D. Hughes, and L. M. Jones, 2021: Airborne sub-pollen particles from rupturing giant ragweed pollen. *Aerobiologia*, **37**, 625–632, https://doi.org/10.1007/s10453-021-09702-x.

Subba, T., M. J. Lawler, and A. L. Steiner, 2021: Estimation of Possible Primary Biological Particle Emissions and Rupture Events at the Southern Great Plains ARM Site. *Journal of Geophysical Research: Atmospheres*, **126**, e2021JD034679, https://doi.org/10.1029/2021JD034679.

——, Y. Zhang, and A. L. Steiner, 2023: Simulating the Transport and Rupture of Pollen in the Atmosphere. *Journal of Advances in Modeling Earth Systems*, **15**, e2022MS003329, https://doi.org/10.1029/2022MS003329.

Sun, T., and Coauthors, 2020: Time-resolved black carbon aerosol vertical distribution measurements using a 356-m meteorological tower in Shenzhen. *Theor Appl Climatol*, **140**, 1263–1276, https://doi.org/10.1007/s00704-020-03168-6.

Taylor, P. E., and H. Jonsson, 2004: Thunderstorm asthma. *Curr Allergy Asthma Rep*, **4**, 409–413, https://doi.org/10.1007/s11882-004-0092-3.

Thien, F., and Coauthors, 2018: The Melbourne epidemic thunderstorm asthma event 2016: an investigation of environmental triggers, effect on health services, and patient risk factors. *The Lancet Planetary Health*, **2**, e255–e263, https://doi.org/10.1016/S2542-5196(18)30120-7.

Tompkins, A. M., 2001: Organization of Tropical Convection in Low Vertical Wind Shears: The Role of Cold Pools. *Journal of the Atmospheric Sciences*, **58**, 1650–1672, https://doi.org/10.1175/1520-0469(2001)058<1650:OOTCIL>2.0.CO;2.

Torri, G., Z. Kuang, and Y. Tian, 2015: Mechanisms for convection triggering by cold pools. *Geophysical Research Letters*, **42**, 1943–1950, https://doi.org/10.1002/2015GL063227.

Twohy, C. H., and M. R. Poellot, 2005: Chemical characteristics of ice residual nuclei in anvil cirrus clouds: evidence for homogeneous and heterogeneous ice formation. *Atmospheric Chemistry and Physics*, **5**, 2289–2297, https://doi.org/10.5194/acp-5-2289-2005.

Twohy, C. H., and Coauthors, 2009: Saharan dust particles nucleate droplets in eastern Atlantic clouds. *Geophysical Research Letters*, **36**, https://doi.org/10.1029/2008GL035846.

Twohy, C. H., and Coauthors, 2017: Saharan dust, convective lofting, aerosol enhancement zones, and potential impacts on ice nucleation in the tropical upper troposphere. *Journal of Geophysical Research: Atmospheres*, **122**, 8833–8851, https://doi.org/10.1002/2017JD026933.

van den Heever, S. C., and Coauthors, 2021: The Colorado State University Convective CLoud Outflows and UpDrafts Experiment (C3LOUD-Ex). *Bulletin of the American Meteorological Society*, **102**, E1283–E1305, https://doi.org/10.1175/BAMS-D-19-0013.1.

——, S. M. Saleeby, L. D. Grant, A. L. Igel, and S. W. Freeman, 2022: RAMS - the Regional Atmospheric Modeling System. https://doi.org/10.5281/zenodo.6869798.

Von Kármán T., 1940: The engineer grapples with nonlinear problems. *Bulletin of the American Mathematical Society*. **46**, 615-683, https://doi.org/10.1090/S0002-9904-1940-07266-0.

Walko, R. L., Couathor 1, and Coauthor 2, 2000: Coupled atmosphere-biophysics–hydrology models for environmental modeling.

Weaver, J. F., and S. P. Nelson, 1982: Multiscale Aspects of Thunderstorm Gust Fronts and Their Effects on Subsequent Storm Development. *Monthly Weather Review*, **110**, 707–718, https://doi.org/10.1175/1520-0493(1982)110<0707:MAOTGF>2.0.CO;2.

Weisman, M. L., and R. Rotunno, 2004: "A Theory for Strong Long-Lived Squall Lines" Revisited. *Journal of the Atmospheric Sciences*, **61**, 361–382, https://doi.org/10.1175/1520-0469(2004)061<0361:ATFSLS>2.0.CO;2.

Werchner, S., E. Gute, C. Hoose, Ch. Kottmeier, A. Pauling, H. Vogel, and B. Vogel, 2022: When Do Subpollen Particles Become Relevant for Ice Nucleation Processes in Clouds? *Journal of Geophysical Research: Atmospheres*, **127**, e2021JD036340, https://doi.org/10.1029/2021JD036340.

Wilson, J. W., and W. E. Schreiber, 1986: Initiation of Convective Storms at Radar-Observed Boundary-Layer Convergence Lines. *Monthly Weather Review*, **114**, 2516–2536, https://doi.org/10.1175/1520-0493(1986)114<2516:IOCSAR>2.0.CO;2.

Wozniak, M. C., F. Solmon, and A. L. Steiner, 2018: Pollen Rupture and Its Impact on Precipitation in Clean Continental Conditions. *Geophysical Research Letters*, **45**, 7156–7164, https://doi.org/10.1029/2018GL077692.

Xu, Q., 1992: Density Currents in Shear Flows-A Two-Fluid Model. *Journal of the Atmospheric Sciences*, **49**, 511–524, https://doi.org/10.1175/1520-0469(1992)049<0511:DCISFA>2.0.CO;2.

——, and M. W. Moncrieff, 1994: Density Current Circulations in Shear Flows. *Journal of the Atmospheric Sciences*, **51**, 434–446, https://doi.org/10.1175/1520-0469(1994)051<0434:DCCISF>2.0.CO;2.

Zhang, R., and Coauthors, 2014: Development of a regional-scale pollen emission and transport modeling framework for investigating the impact of climate change on allergic airway disease. *Biogeosciences*, **11**, 1461–1478, https://doi.org/10.5194/bg-11-1461-2014.